# Performance of a Plasma Torch
# With Hydrocarbon Feedstocks for Use in Scramjet Combustion

by

John L. Prebola Jr.

Thesis Submitted to the Faculty of the
Virginia Polytechnic Institute and State University
in partial fulfillment of the requirements for the degree of

**MASTER of SCIENCE**

in

Aerospace Engineering

Approved:

Dr. Joseph A. Schetz, Chairman

Dr. Walter F. O'Brien

Dr. Charlie L. Yates

August, 1998

Blacksburg, Virginia

# Performance of a Plasma Torch With Hydrocarbon Feedstocks for Use in Scramjet Combustion

by

John L. Prebola, Jr.
Committee Chairman: Dr. Joseph A. Schetz
Aerospace an Ocean Engineering Department

## (ABSTRACT)

Research was conducted at Virginia Tech on a high-pressure uncooled plasma torch to study torch operational characteristics with hydrocarbon feedstocks and to determine the feasibility of using the torch as an igniter in scramjet applications. Operational characteristics studied included electrical properties, such as arc stability, voltage-current characteristics and start/re-start capabilities, and mechanical properties, such as coking, electrode erosion and transient to steady-state torch body temperature trends. Possible use of the plasma torch as an igniter in high-speed combustion environments was investigated through the use of emission spectroscopy and a NASA chemical kinetics code.

All feedstocks tested; argon, methane, ethylene and propylene, were able to start. The voltage data indicated that there were two preferred operating modes, which were well defined for methane. For all gases, a higher current setting, on the order of 40 A, led to more stable torch operation. A low intensity, high frequency current applied to the torch, along with the primary DC current, resulted in virtual elimination of soot deposits on the anodes. Electrode erosion was found to multiply each time the complexity of the hydrocarbon was increased. Audio and high-speed visual analysis led to identification of 180 Hz plasma formation cycle, related to the three-phase power supply. The spectroscopic analysis aided in the identification of combustion enhancing radicals being produced by the torch, and results of the chemical kinetics analysis verified combustion enhancement and radical production through the use of a basic plasma model. Overall, the results of this study indicate that the plasma torch is a promising source for scramjet ignition, and further study is warranted.

# Acknowledgements

I would first like to thank my advisor, Dr. Joseph Schetz, for giving me the opportunity to work on such an interesting project. His guidance, insight and ability to draw upon a vast amount of experience were vital during all aspects of this research. I am also grateful to my committee member, Dr. Walter O'Brien, for his excellent knowledge and understanding of plasma torch operation, with which we were able to quickly overcome many problems during testing. My thanks also go out to Dr. Charlie Yates, not only for serving on my committee, but for his instruction on propulsion systems which helped me to see the "Big Picture" of what this research will accomplish.

This project would not have been possible without the financial and technical support of the people at Phoenix Solutions Inc.. The two-way transfer of knowledge gained from testing helped to clear many roadblocks. I am also thankful to Dr. Casimir Jachimowski for giving me a better understanding of chemical kinetics and taking the time to help me run my test cases.

Thanks are also in order for the AOE and ME shop guys, like Gary, Bruce, Greg and Bill who continually reshaped and rewired the torch and equipment after tests resulting in "limited success".

I must also thank all the friends I have made in Blacksburg for the many memories they have given me. Without those athletic and social activities I may not have made it.

Most importantly I appreciate all the support from my family and friends back home, throughout my academic career. I especially thank my parents, whose guidance and caring have been beyond words.

# Table of Contents

# List of Tables

# List of Figures

# I. Introduction and Background

**History of Scramjets:**

As early as the late 1950's there was interest in combustion at supersonic speeds. When a supersonic air stream is lowered to subsonic velocities before combustion can take place, there are efficiency losses due to shocks and extreme temperatures and pressures [1]. To overcome this problem, the flow within a combustor can be decelerated, but remain supersonic while the fuel is injected and burned. The basic idea consists of an inlet, combustor and nozzle, as in

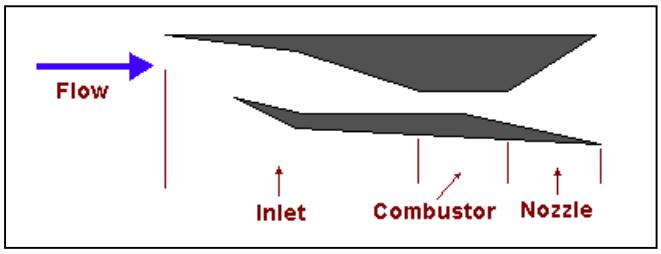


**Figure I.1: Basic Scramjet Engine**

Figure I.1 which has no moving parts. Due to the high static pressure rise generated at the inlet and large static temperature increase across the combustor, a net positive thrust can be achieved [2]. While this may sound promising, there are various problems associated with this type of engine. One drawback is the fact that an engine of this type is not capable of starting itself from zero velocity, as with turning the turbine-compressor in a turbojet engine, therefore it needs an additional propulsion system to raise its speed above about Mach 4. Another hindrance in the development of this type of propulsion system is the short fuel residence time within the combustor due to the high flow speed through the engine.

Efforts to overcome this problem have been ongoing since the 1960's at NASA, particularly at the Langly Research Center (LaRC), the Applied Physics Lab of John's Hopkins University and elsewhere in the US and overseas. Experimental research began with the Hypersonic Research Engine project in the mid 1960's which developed into the Airframe Integrated Scramjet Concept [3]. Later, in the late 1970's and early 80's, base scramjet research was conducted with wind tunnel experiments and computational fluid dynamics (CFD) analysis. This research helped in the development of the three-strut, strutless parametric and step-strut engine design concepts that enhanced fuel injection and fuel-air mixing at supersonic flow

velocities in the combustor [4]. In the mid 1980's, funding and research began on the National Aero-Space Plane (NASP), which was to take and build on the knowledge gained from earlier experiments and construct an operational scramjet engine. Both Pratt & Whitney (P&W Engine C) and Rocketdyne (Hydrocarbon-Fueled Scramjet) designed and tested engines during this period and after NASP funding was cancelled in 1995 [5, 6]. Currently work is being done on the Hyper-X scramjet engine design, which is intended to take hypersonic, air-breathing technology from the ground to actual flight tests by early 2000 [7].

Further work was done at various institutions to continue scramjet research and solve the problems associated with it. Some of these proposed solutions consisted of integrating a rearward leaning step in the combustor to enhance mixing [8, 9], adding triple wedge struts in a rectangular engine configuration that provide multiple fuel injection planes, burning of a fuel-rich mixture in a small cavity with a plasma torch to introduce combustion enhancing radicals into the main stream [10], and a configuration of pilot and main fuel injectors combined with an uncooled plasma torch igniter [9].

In most scramjet testing, hydrogen has been the fuel of choice, however there has been some interest in supersonic combustion using hydrocarbon fuels. While hydrogen is advantageous as a scramjet fuel due to its low molecular weight, cooling capability, thermal stability and high reactivity, it requires special handling techniques and storage facilities [11]. Also, the low density requires a large volume to hold a useful amount of fuel, which presents problems in the design of small vehicles. Hydrocarbon fuels, on the other hand, are presently used in the majority of military and commercial engines and facilities already exist to sustain engines operating on these fuels, but hydrocarbons have proven difficult to achieve ignition and combustion in supersonic airstreams [12].

As early as the late 1960's interest was focused on plasma torches for ignition purposes [13]. Early tests focused on ignition in internal combustion engines and fuel lean mixtures and resulted in more enhanced penetration into the fuel/air mixture than spark ignition and an increased burn velocity [14, 15]. Also plasma torches have been found to be reliable ignition aids in low speed flows, up to Mach 2, since they produce atoms, molecules and excited species that accelerate the combustion reaction process [16, 17].

The research conducted at Virginia Tech focused primarily on the operation of a plasma torch with methane, ethylene, and propylene in an effort to study torch operational characteristics and possible implementation of the torch as an igniter in supersonic combustion applications using hydrocarbon feedstocks.

**Emission Spectroscopy:**

During the time of Isaac Newton in the late 1600's the idea of dispersed light producing a defined spectrum was just becoming known. It wasn't until 1826 that W.H. Talbot determined that when a specific homogeneous ray of any color results from passing the light of a flame through a spectrum, there exists a specific chemical compound based on that color [18]. Later developments resulted in more precise dispersion instruments than prisms, such as gratings. A reflection grating consists of a series of identical grooves equally spaced on a reflective surface that can be either plane or concave [19]. The basic characteristics of a grating are the dispersion and resolving power, based primarily on the number of grooves per millimeter and the groove angle. The resulting dispersion pattern can be a line or series of lines separated by small "dark" areas caused by destructive wave interference [18].

To detect a particular wavelength being dispersed off the grating, several detectors are commonly used. These include photographs, photomultiplier tube, semiconductors and thermoelectric detectors. A photomultiplier tube is a vacuum photo-emissive diode combined with a low-noise emission electron multiplier. The cathode emits electrons upon irradiation which are collected by an anode and therefore pass current. This current is passed through a series of load resistors and develops a photovoltage that can be read by instrumentation such as a multimeter or computer data acquisition system.

Plasmas have been found to be excellent radiation sources for use in emission spectroscopy, as a result of their temporal stability and ability to emit spectral lines that are not excited in a typical flame [20]. In hydrocarbon plasmas, the ionized gas produces more excited atoms and molecules than in a flame, so the species are more easily detected and more abundant [21]. In relation, there have been several studies conducted to better understand how hydrocarbon plasmas react in both the subsonic and supersonic flow regimes. These experiments helped identify the location of the highest concentrations of a particular species, as in the

boundary layer analysis of nitrogen-methane plasma flow [22], which can lead to better placement of fuel injectors.

In addition, knowledge of species present in the flow can aid in the kinetic modeling of high-speed reacting flows. As in the analysis of ethylene oxidation, where a full set of 505 reactions and 78 species was reduced to 9 species and 8 reactions, an experimental data set is required to test the validity of a reduced scheme [23]. The reduced reaction set can then be used to verify experimental results and save time in theoretical analysis of innovative combustor configurations.

## II. Equipment and Setup

The following section describes the equipment and arrangement used in the Virginia Tech Plasma Torch Lab to conduct tests with a plasma torch using hydrocarbon feedstocks. The lab setup can be divided into five sections: plasma torch, flow system, data acquisition, power system and safety equipment. Although the arrangement of the lab varied throughout the testing process, the setup described below is considered standard. Any deviation from this setup will be listed and explained for each test sequence, as applicable.

### Plasma Torch

A plasma torch consists of a negatively charged cathode and a positively charged anode separated by a small gap. Between the gap a particular gas or mixture of gasses is flowing at a

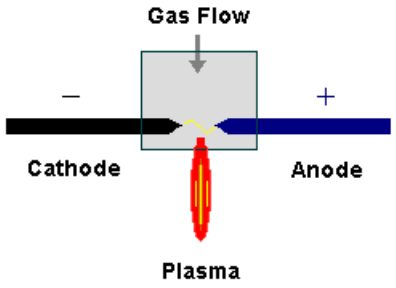


**Figure II.1: Basic Plasma Torch**

specific pressure, which limits the diameter of the plasma jet. The type and composition of the feedstock, the flow pressure at the electrodes and arc gap determines the required voltage differential between the electrodes to initiate an electric arc. In monatomic gases, such as argon, at low pressure, the required breakdown voltage is on the order of 150 V.

The Virginia Tech plasma torch uses electrodes made from 2% thoriated tungsten. To produce thoriated tungsten, pure tungsten is contaminated with thorium, an electropositive element, using a special heat treatment. This process enhances the electron emission ability of pure tungsten [24]. Tungsten and its alloys are often used in high temperature environments, since they provide an exceptionally high melting point (≈3900 K) and good electrical

conductivity at high temperatures. This is in part due to its body-centered-cubic crystalline structure.

Its ability to withstand high temperatures and still maintain desirable chemical, mechanical and electrical properties make tungsten desirable for many different applications, including various types of electrodes. A study of arc discharges [25] showed that among six different materials tested, thoriated tungsten and pure tungsten had the lowest anode mass loss rates. Even though thoriated tungsten had a slightly higher mass loss rate than pure tungsten, the electrodes were constructed from it because of its machineability.

Figure II.2 is a graph of tungsten thermal conductivity versus temperature [26]. The Virginia Tech plasma torch usually operated with a body temperature between 450-600K with

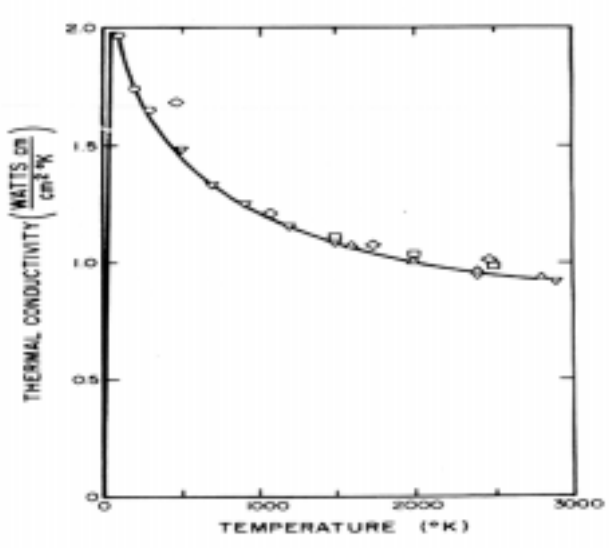


**Figure II.2: Tungsten Thermal Conductivity**

the anode bulk temperature being slightly higher. Electrical conductivity, the ability of a material to allow electric current pass through it, is one way of measuring how much damage might be incurred if an arc were to strike it, as in the case of an electrode. High thermal conductivity and heat tolerance would allow the material, in this case, tungsten, to function with minimal loss in mass while operating as an electrode. Tungsten has long been used as a material for manufacturing electrodes and is an ideal choice for use in a plasma torch.

The Virginia Tech plasma torch electrode geometry allows the torch to operate in two different modes depending on the voltage available. The modes are characterized by where the

arc attaches to the anode. It can operate in either a high-voltage or a low-voltage mode, shown in Fig II.3[27].

**High Voltage Mode**

**Low Voltage Mode**

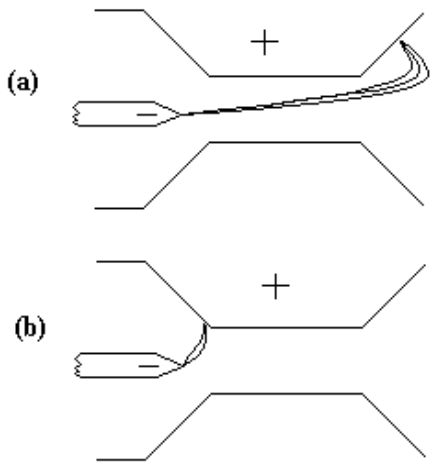


**Figure II.3: Torch Voltage Modes**

The high voltage mode, which is how Virginia Tech plasma torch usually operates, is shown in Fig. II.3(a). In this mode, the arc passes completely through the anode constrictor and attaches itself on the diverging section of the nozzle. In the low voltage mode, Fig. II.3(b), the arc attaches on the converging section of the nozzle. The low voltage mode is known to be most damaging to the anode. Pressures at the point of arc attachment for the low voltage mode are higher than for the high voltage mode. Higher pressure produces a smaller arc cross sectional area and therefore a higher heat flux [27]. The amount of electrode wear is directly proportional to the rate of heat flux.

To further promote healthy torch operation and minimal electrode loss, arc rotation was introduced through the use of a flow swirler located upstream of the throat (Fig. II.4.a - part v). Arc rotation is necessary to insure even wear of the electrodes, which helps to maintain the shape of the nozzle. Multiple swirler designs were tested before the optimum configuration was determined [27].

Unless a test required a specific torch modification, such as arc gap adjustment, the plasma torch was set up identically for each test. First, the electrodes were replaced if they showed sufficient wear to be inadequate for the current test series. Gas seals and thread sealants were replaced every time the torch was disassembled to ensure quality operation. The torch was then reassembled following the schematic shown in Fig. II.4.a.

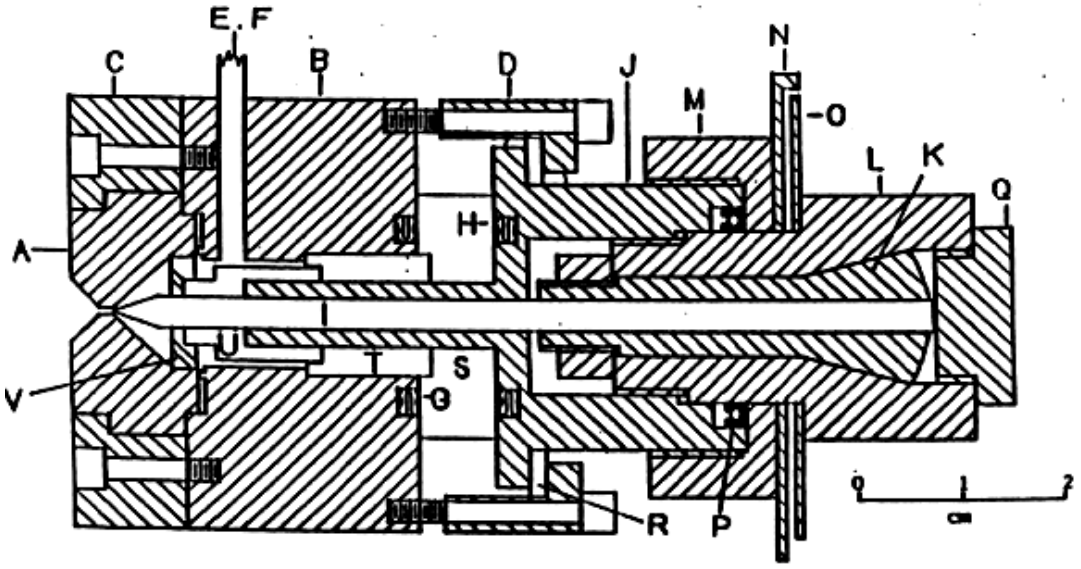


**Adjustable Gap Plasma Torch** A, anode; B, body; C, anode holder; D, pressure ring; E, gas inlet; F, pressure tap; G,H, E-ring seals; I, cathode; J, cathode alignment piece; K, collet; L, cathode adjustment knob; M, gland cap; N, mounting bracket; O, angle indicator; P, dynamic seal; Q, end cap; R,S, insulators; T, alignment piece; U, insulator; V, flow swirler

**a.**


**b.**

**Figure II.4: Plasma Torch Schematic and Components**

Axial gap adjustment was made by the use of the plasma torch's micrometer drive and a multimeter. The multimeter was connected across the anode and cathode to check for continuity. The cathode was forced to make contact with the anode by adjusting the micrometer drive. The cathode was then backed out until continuity was broken. From this point, the cathode was backed out an additional 0.178mm (101° on the micrometer drive) as prescribed by Stouffer [27]. Once the gap adjustment was made, the torch was bolted onto a Plexiglas stand in the test cell used to electrically isolate the torch from lab equipment. The torch body thermocouple, and inlet gas and pressure lines were then connected. With the power off, electrical connections were made by the use of jumper cables. One cable was attached to the pressure line (anode) and the other to a steel ring (Fig. II.4-b - part 12), specially designed for this type of power connection. From this point the feedstock was set and run at the desired flow rate and then the power supplies were turned on. Plasma torch ignition was initiated by a burst of high frequency current. For tests requiring the collection of voltage and current data, the voltage and current leads were connected to the data acquisition system after the high frequency starter was turned off. Plasma torch power levels ranged from 1.0-3.5 kw for both methane and ethylene. Each gas had an average power of 2.2 kw. Although both feedstocks had the same range and average power, ethylene tended to oscillate between 1.0-3.5 kw more frequently than methane.

## The Flow System

The flow system is responsible for delivering the feedstock to the plasma torch at the correct flow rate. It consists of the gas storage cylinders (argon, methane, ethylene and propylene), dual-stage regulators, tubing and fittings, two mass flow meters, a dual-channel flow controller and the torch itself (Fig II.5).

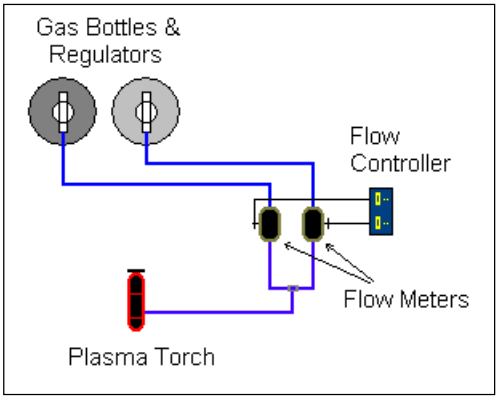


**Figure II.5: Flow System Schematic**

Four separate gases were used to test the plasma torch operation: argon, methane, ethylene and propylene. They were stored in high pressure gas cylinders provided by a local vendor. Flow pressure was controlled by Victor® dual-stage regulators. They allowed the flow pressure to be adjusted from 0-3.45Mpa (0-500 psig). Pressure was generally set at 0.69-0.83MPa (100-120 psig). The regulators were custom designed for the gases listed above.

All tubing in the flow system was made from 6.35mm (0.25in) Nycoil® tubing connected by 6.35mm (0.25in) Swagelock fittings. The particular type of Nycoil® tubing used was made from flexible nonconductive material with an operating pressure of 1.72Mpa (250 psig) and a burst pressure of 6.9Mpa (1000 psig). When both argon and a hydrocarbon gas were fed through the torch, the gases were combined using a T-fitting and then passed through two feet of 6.35mm (0.25in) tubing to assure adequate mixing.

Two Sierra Series 840M mass flow meters were used to control the amount of flow to the torch. One flow meter was factory calibrated for argon and had a range of 0-20 SLPM. The second flow meter was factory calibrated for use with methane and had a range of 0-30 SLPM. When ethylene or propylene was used in place of methane a calibration factor was needed to

adjust for the different material properties of ethylene. This calibration correction is shown in the following equation,

$$Q_2=Q_1*K$$

$$K=[N_1/(\rho_1 C_{P1})]\ [(\rho_2 C_{P2})/N_2]$$

where $Q_2$ is the actual ethylene or propylene flow rate, $Q_1$ is the flow rate reading on the mass flow controller and K is the calibration factor determined using data provided by Sierra Instruments. For ethylene, K=1.20 and for propylene, K=0.56. The flow meters are shown in Figure II.6. The flow meter in the foreground is used to control the flowrate of argon, while the one in the background controls the hydrocarbon flowrate. Both flow meters rely on a large-diameter thermal mass flow sensor, which is virtually clog-proof. They utilized precision analog circuitry with a five-breakpoint linearizer, providing highly accurate calibration ability. Each flow meter was accurate to ±1% of full scale. The response time was generally one second to achieve ±2% of the required flow rate.

**Figure II.6: Mass Flow Meters**

A 902C Dual-Channel Flow Controller, manufactured by Sierra Instruments, was used to control the two mass flow meters. It was factory calibrated to operate with the flow meters. The flow controller is shown in Figure II.7.


**Figure II.7: Mass Flow Controller**

The face of the flow controller consists of a digital readout, readout select switch, two flow control potentiometers, rotary channel select knob and power switch. The flow control potentiometers allow the user to adjust the amount of flow through the flow meters. The readout select switch changes whether the digital readout displays actual flow rate or set flow rate for the channel chosen by the rotary channel selection knob. Control signals were sent to the flow meters using two-way parallel cables. Electrical connections on the back of the flow controller provided 0-5 volt outputs which could be used to send signals to the data acquisition system. These signals were then converted into flow readings on the computer monitor.

## The Data Acquisition System

The data acquisition system was constructed to collect and process the data required to conduct the testing series. The system consists of an IBM 486 PC, a National Instruments™ AT-MIO-16E-10 multifunction analog and digital I/O data acquisition (DAQ) card, 3 analog signal conditioning modules, LabVIEW 4.0 software, Model 82-020 Series 0.5 Meter Ebert Scanning spectrometer, a Burle 1P28B Photomultiplier tube (PMT) in housing, current shunt, hand-held current meter, Genisco Tech 0-0.690Mpa (0-100 psia) pressure transducer and Measurements Group 2310 signal conditioning amplifier, analog pressure gage, type K torch body

thermocouple and a video camera. The three signal conditioning modules have ±50mV, ±10V and a Type K thermocouple inputs with a ±5V output on each (Fig II.8).

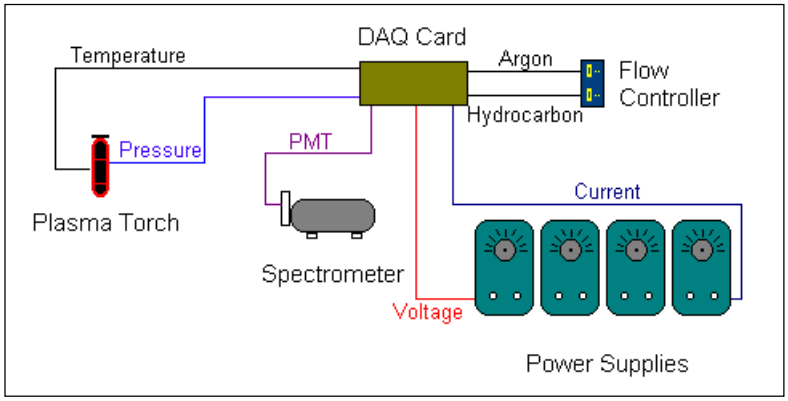


**Figure II.8: Data Acquisition Schematic**

For a majority of the tests, the thermocouple, current shunt and power supply voltage were connected to the analog signal conditioning modules. This provided signal filtration and isolation of the DAQ card and PC from any unanticipated surges in the power supply system. The pressure transducer and flow meter outputs were pre-conditioned and, therefore, run directly into the DAQ card through the use of a CB50 connector block (Fig. II.9).

**Figure II.9: Data Acquisition Hardware**

Spectrographic tests conducted with the Virginia Tech plasma torch utilized a 0.5 meter Ebert scanning spectrometer (Fig. II.10) with a diffractive grating of 1180 grooves/mm. The full scanning range of the spectrometer was from 1900 to 9100 Angstroms (Å), with a


**Figure II.10: Spectrometer Setup**

resolution of approximately 1Å. A two foot length of PVC pipe was aimed at the plasma jet in an effort to capture only arc light as it entered the spectrometer. Between the PVC pipe and the entrance slit, there were two Oriel absorptive neutral density filters. These filters had an optical density of 3.0 and a range of sensitivity as seen in Fig. II.11.

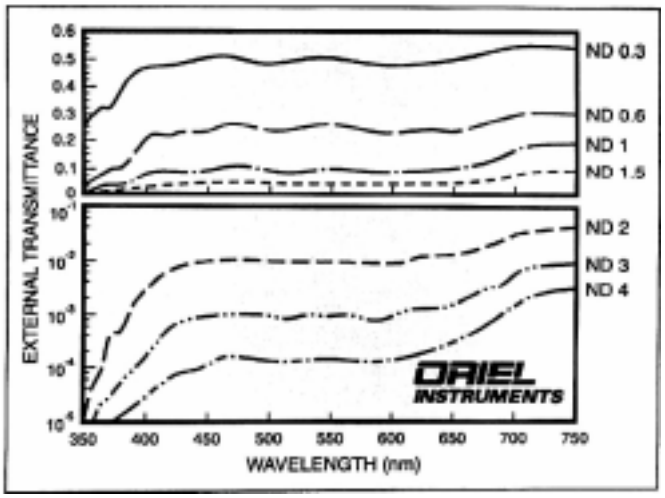


**Figure II.11: Filter Transmittance from Oriel Data Sheet**

It was noted that transmittance dropped off sharply below 3500 Å.

After the filters, the remaining light traveled through the spectrometer, was dispersed by the grating and left through the exit slit. Attached to the exit slit was the Burle photomultiplier tube (PMT). This PMT, powered by a 15V supply, had a variable gain potentiometer that was set depending on output intensity. In some cases after a few tests were conducted, the gain had

to be increased to get the same resolution as the previous runs due to desensitization of the PMT. A graph of the spectral response characteristics is given in Fig. II.12.

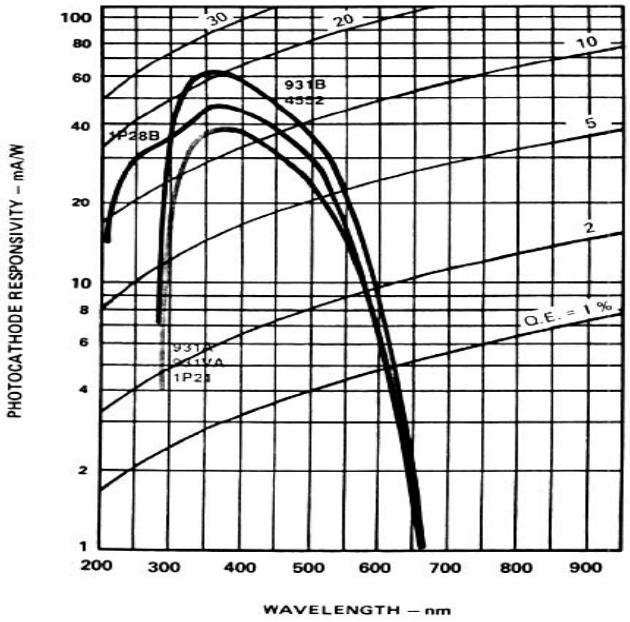


**Figure II.12: Photomultiplier Tube Response Characteristics**

A simple resistor was connected across the output leads of the PMT, so that the voltage drop across the resistor could be measured. Since the voltage drop across the resistor was on the order of 0 to 50 mV, the signal conditioning module that was used to measure power supply current was chosen to read the PMT output.

It was necessary to check the calibration of the spectrometer to insure that the wavelength counter on the instrument was correct. A 200w Oriel mercury arc lamp was chosen, since a mercury arc has well defined peaks at 2491 Å, 4046 Å, 4358 Å and 5461 Å. After the calibration run was completed, the spectral irradiance data sheet for the Oriel lamp matched the computer output of the PMT to within 2.0 Å. Also noted was the fact that the 2491 Å peak was registered by the DAQ system despite the neutral density filters resolution dropping off at 3500 Å.

As a check to the DAQ system, the analog pressure gage and hand-held current meter were continually compared with the computer output of the pressure transducer and shunt channels. This verification of the DAQ system was performed prior to each test series to insure correct data collection.

For the first few tests, a video camera was used as form of data collection and validation. Replay of the tape at low speed helped to qualitatively evaluate torch operation in a slower time scale. Also, the steps of the testing procedure could be retraced to see if any step was completed out of sequence, or if a more informative sequence could found.

## Power System

The power system was used to generate and deliver sufficient power to ignite and sustain the plasma torch. It consisted of four welding units connected in series and one high frequency starter box. This configuration provided an open circuit voltage of approximately 270 volts(V). The plasma torch could be run in either DC or high frequency mode due to the available power and flexibility of the system.

Two of the four welding units are shown in Fig. II.13 Each one is a Miller Electric Constant Current, DC, SR-150-32. They have an open circuit voltage of 67 V and can produce 5-150 amps(A). Most tests were conducted at 30 A or below, with the norm being 25 A. Each unit is equipped with a high frequency starter. These starters were used in early tests to ignite the torch, but they proved to be problematic because of the great intensity of the high frequency signal produced, so an external high frequency starter box with variable high frequency ability was purchased to alleviate the problem.

**Figure II.13: Power Supplies**

The external high frequency starter box used in all but the initial tests is shown in Fig. II.14. The Miller Electric HF-251D-1 is equipped with a high frequency intensity selection knob

(0-100%), remote switch and start/continuous selection switch. All tests requiring the use of high frequency current were conducted at intensity levels of 5% or below and run on continuous high frequency. Applying a burst of high frequency to the plasma torch and then turning off the HF-251D-1 started DC tests.


**Figure II.14: High Frequency Starter Box**

## Safety Equipment

When conducting any test resulting in plasma or flame generation, safety equipment becomes a necessary consideration. Measures were taken to ensure the safety of those in the immediate area when the plasma torch was in operation. Any form of arc will generate large amounts of UV that must be shielded to prevent eye and skin damage. A 12.7mm (0.5 in) thick transparent Lexan® sheet was placed in-between the plasma torch test cell and the control room. This sheet had three purposes. First, it needed to be transparent to allow a clear view of the plasma torch operation. It also provided a moderate amount of UV protection. Most importantly, the Lexan® sheet provided superior blast protection to that of standard glass or Plexiglas due to its high resistance to shattering. Also, when directly looking at the plasma torch while it was in operation, a welding shield with a tint level of 12.0 was used.

The test cell itself also had safety measures built into it. The main portion of the test cell was built from a 0.254m x 9.5mm (10”x3/8”) steel pipe and located on the outside of the building. It had a 90° elbow with a three foot extension to force the exhaust gases up above head

level. It was also equipped with a rain hood.  A fire resistant fabric used to keep out weather and block any light that might alter spectroscopic readings enclosed the rest of the test cell. A picture of the plasma torch in the test cell is shown in Fig. II.15.

**Figure II.15: Plasma Torch in Test Cell**

## III.A: Plasma Arc Stability

It is important to have stability in the arc to insure consistent operation and less electrode wear. With consistent operation and less part wear, there can be a large cost savings in fewer redundancies and parts replacement. In addition, knowing how stable the arc is operating can significantly help to predict torch component life.

If the arc is unstable, there may be unpredictable ignition and a strong possibility of flameout. Also, a misdirected plume can result in "hot spots" in the engine that could result in catastrophic failure. With that in mind, finding stable and unstable arc modes is very important for the present application.

Arc stability can be characterized through parameters such as current level, electrode emission, jet direction and fluctuations in the flame plume. An arc that has variations in current of more than a few amps may be fluctuating between two or more operating modes. The inability of the arc to settle in a specific mode may be attributed to the current level setting on the power supplies, the gas flow rate or the electrode gap size. In any case, an unstable arc is more likely to terminate than one that is stable.

Another way of determining if arc stability exists is if electrode emission is low. At the atomic level, the stream of electrons leaving the cathode continuously impacts the anode. If the electron stream is steadily circulating with the swirling gas flow, minimal electrode emission occurs. However, when the arc jumps sporadically, the sudden flow of electrons from an isolated location dislodges pieces of the electrodes.

The direction of the plasma jet is also an indicator of arc stability. During stable operation, the jet projects outward perpendicular to the exit face of the torch. This is a result of the internal flow swirler and gas flow direction as determined by the design of the torch. Occasionally, the jet is slightly off center due to anode throat wear from previous testing, but it is still maintaining a stable operating mode. Any time there are intermittent direction changes in the jet, this indicates that some aspect of the arc is transitioning through instability.

A fluctuating flame plume may indicate instability, since a flame plume is present only when specific combustion reactions are taking place. As different reactions are taking place and

the plume varies from existent to non-existent, an unstable transition between operating modes is occurring. A strong steady plume may suggest that the arc is operating in a very stable mode.

## Test Setup and Procedure

The standard equipment setup was used except for disconnecting the data acquisition system prior to torch startup and maintaining a constant 5% continuous high frequency intensity on the HF starter.

Both methane and ethylene were tested using the same procedure. An initial current of 14% (about 21 A) was set on all four power supplies. The HF starter was set at 5%, and the flow controllers were run at a constant flow rate of 25 SLPM. The continuous run mode on the HF starter was turned on, which started the plasma torch. After one minute, all four power supplies were reduced 2%. The "one minute operation/reduce 2%" procedure was sequentially repeated until the torch ceased operation. Throughout the tests, notes were taken on how much electrode emission was occurring, plasma jet direction and plume size.

## Results and Discussion

Testing was first performed using methane. At higher current settings there were small amounts of electrode emission (about 5 glowing particles per second). As the current setting was reduced to near 10% current, cycling between operating modes began. This cycle initially had a 20mm plasma jet that slowly reduced in size to approximately 10mm over a period of 5 seconds. At that point, the jet would rejuvenate to the 20mm initial size. Throughout the cycle, minimal electrode emission was present. A very small (5.0mm) stable jet was produced in the range of a 7% current setting, and at about 5% current setting the torch went out.

Ethylene had electrode emission of about 30 particles per second at higher current settings. Despite the high emission, the arc appeared to be stable at the standard operating conditions, with a steady jet and straight plume as shown in Fig. III.A.1.

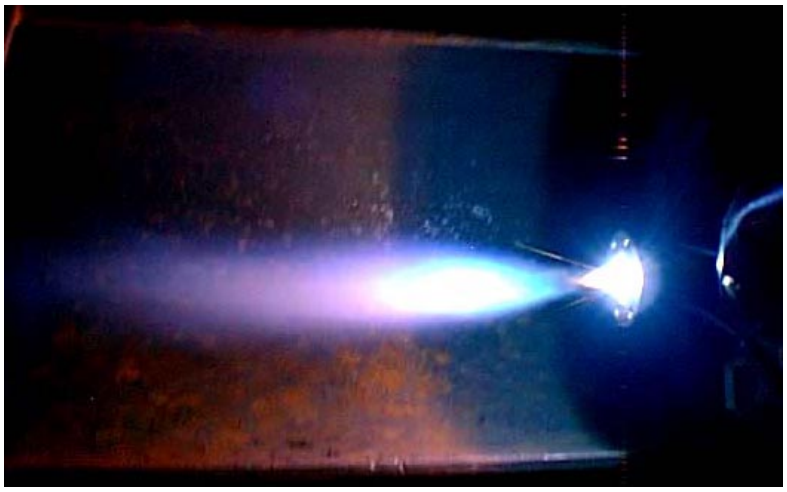

**Figure III.A.1: Stable Ethylene Operation**

Again, the jet size decreased with decreasing current. At 8% current, there was approximately a 2.0mm jet that was operating highly unsteadily, but with less electrode emission. The jet direction was erratic and the flame plume was small and in bursts. As soon as the current was decreased more, the torch ceased operating.

## Final Remarks

Overall, the arc appeared more stable at the higher current settings, although methane did seem to have stable operation near 7% current. Only ethylene had high amounts of electrode emission, particularly at the upper current settings. This emission reduced with reduced current, but combined with the unsteady jet and flame plume, the lower current settings were not favorable for extended torch life. Between 8-10% current, both methane and ethylene had unstable operation.

## III.B: Torch Voltage and Current Characteristics

An important aspect of plasma torch operation is the variation in arc voltage for different current level and gas flow rates. It is necessary to look at trends in order to locate favorable operational configurations. Knowledge of such modes permits torch operation with the least power required to complete the mission.

Some previous work on methane arcjets has been reported [11] resulting in V-I characteristics as seen in Fig. III.B.1. It was concluded that voltage was insensitive to variations in current at the given mass flow rate of 87 mg/sec.

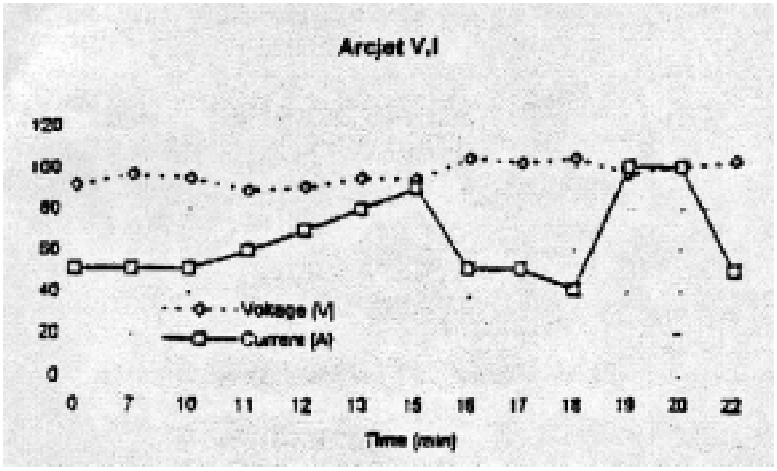


**Figure III.B.1: [11] Arcjet V-I Characteristics**

### Test Setup and Procedure

The test setup was similar to the standard configuration with the following exception. During startup, the power supplies were disconnected from the data acquisition (DAQ) system. Once the torch was operating, the high frequency (HF) starter was turned off, and the power supplies were connected to the DAQ system.

Testing began with setting the hydrocarbon flow controller at a flow rate of 30 SLPM of methane. The power supplies were set to 30% current (about 45A), and the HF starter was set to 5%. With the flow rate, current and HF ready, the power supplies were turned on, and the HF starter was activated. As soon as the torch was started, the HF starter was turned off, and the power supplies were attached to the DAQ system. Immediately following connection, the DAQ system was activated. After an interval of 5 seconds, each of the four power supplies was turned down 4%. The 5 second pause and 4% reduction was repeated until a 6% current setting was reached on the welders.

The above procedure was repeated for a total of seven methane flow rates ranging from 30 SLPM to 12 SLPM in 3 SLPM increments. Five ethylene tests were completed ranging from 36 SLPM to 21.6 SLPM in approximately 3 SLPM increments. The odd testing increment for ethylene was due to a calibration factor that had to be applied to the output of the flow controller.

## Results and Discussion

After testing was complete, the voltage and current data was plotted to see if any trends could be found. In all figures, the purple curve is actual current (A), the magenta curve is actual voltage (V), and the x-axis is time (sec). There are $9^{th}$ order curve fits (light blue for voltage and green for current) fitted through the data, which help to show trends in the data.

Figure III.B.2 contains graphs for methane at four flow rates: 30, 24, 18, and 12 SLPM. In all four graphs, the current is initially near 45A, which is consistent with the setting on the power supplies. For 30 SLPM in Fig. III.B.2-a, the imposed decrease in current setting over the first 20 seconds is not registered. However, there is a steady drop in voltage, which may indicate that the arc is more easily maintaining itself in a specific operating mode. Between 20 and 40 seconds, there is a continual drop in current to approximately 20A. At 40 seconds, the power supply settings had been reduced to 14%, resulting in a current of 21A. Over this range, the voltage returns to its high level near 80V. Beyond 40 seconds, the current remains in the 20A range, and the voltage is decreasing, again indicating a tendency to maintain an operating mode.

There is more variation in the curves of Fig. III.B.2-b for 24 SLPM. The initial current is within the range of the setting on the power supplies, but the voltage is initially much lower than the 30 SLPM run. As the current setting is decreased, there is an increase in current and a

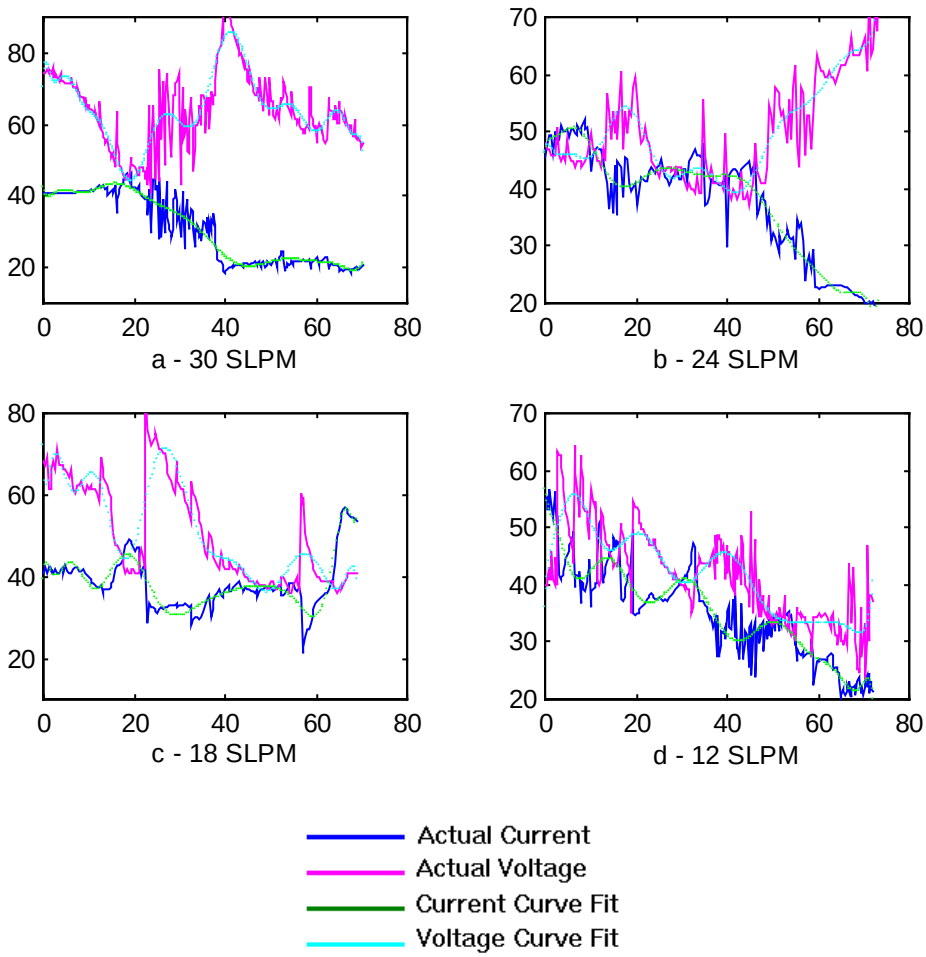


**Figure III.B.2: V-I Characteristics for Methane**

decrease in voltage. This indicates that the torch may be trying to "jump" to a stable operating mode at a slightly higher current level. As the second drop in current setting takes place, the current values drop down to the 40A range. This is similar to the 30 SLPM case. The voltage also drops to 40V at about 20 sec. As the current setting is decreased further, the 40A operating mode is maintained. The voltage once more remains low over this range indicating preference

for this operating mode. Near 50 seconds, the current decreases with current setting towards the 20A operating mode while the voltage increases. The increase in voltage may suggest that continuing to operate at the 20A mode is becoming more difficult.

Similar to the 30 SLPM run, the data for the 18 SLPM run in Fig. III.B.2-c starts out at the 40A operating mode with a high voltage. As the current setting is decreased, the voltage drops, requiring less power to operate at that mode. Torch operation appears to become unstable as the arc tries to maintain the 40A mode with further decreases in power supply current setting. At 40 seconds, however, the voltage drops to 40V and the 40A mode is maintained. Rapid fluctuations in the current and voltage near 60 seconds may indicate an inability to operate at any stable mode.

At low flow rates near 12 SLPM (see Fig. III.B.2-d), the current never seems to stabilize at an operating mode. There is a cyclical decrease in the voltage and current over the full test time. It is possible that the low flow rate is not strong enough to support the arc swirl, therefore it is easier for unstable arc jumps to occur.

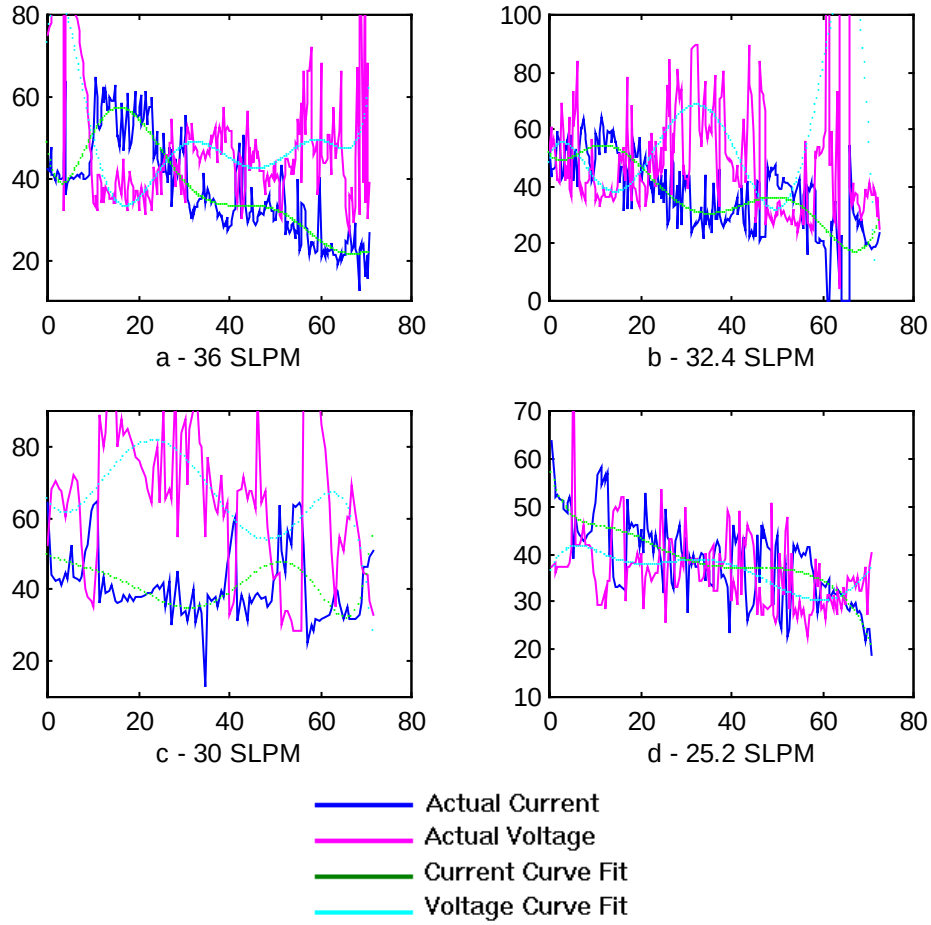


**Figure III.B.3: V-I Characteristics for Ethylene**

The results of the ethylene tests are given in Fig. III.B.3. Unlike the methane tests, the voltage and current data fluctuates over a wider band for ethylene. In the first run at 36 SLPM, Fig. III.B.3-a, the 40A operating mode is again produced, but with large variations in voltage. As current setting is decreased, there is a current jump to near 55A, yet the voltage remains in the 40V range. It appears that the jump to the higher operating mode did not affect the voltage. Past 30 seconds, the current and voltage curves steadily decrease, but diverge cyclically, possibly indicating a near equal pull towards two different modes.

There is a higher starting current of 50A in the 32.4 SLPM run in Fig. III.B.3-b. As the current setting is decreased, there is an increase in current to the 55A mode. Operation in this

mode begins to drop off near 20 seconds, and current steadily decreases until 30 seconds. From the 55A operational mode until the 30 second point, the voltage steadily rises. This increase in voltage indicates a greater effort by the torch to operate in that mode. After 30 seconds, the voltage begins to drop, and the current increases to near the 40A operating mode. The decrease in power supply current setting near 60 seconds causes large current and voltage fluctuations, implying inability to operate in any stable mode.

For 30 SLPM in Fig. III.B.3-c, voltage and current are highly variant over the first 10 seconds of the test. After 10 seconds, the current averages near the 40A operating mode, until about 30 seconds, when again the variations in current become large. The voltage maintains a high and erratic value over the entire test, indicating that no stable operation was achieved.

At 25.2 SLPM, Fig. III.B.3-d, current and voltage are steadily falling throughout the test. There does not appear to be any leveling off at an operating mode, but at 18% current setting, about 30 seconds, the curves cross over the 40 A operating mode and level off for a brief period. After 60 seconds, there is another crossover of the curves at 35A and 35V designating another possible stable mode.

**Final Remarks**

Considering the voltage and current output from the torch, there appeared to be a correlation between the two. However, this conflicts with the results of the Hruby [11] arcjet experiments seen in Fig. III.B.1. In the Virginia Tech plasma torch, methane appeared to have two stable operating modes, 40A and 20A, at which it repeatedly tried to operate. At the three higher flow rates, operation in the 40A mode near 20 seconds required the least power to operate, since the voltage dropped to the level of the current. The 20A mode required more voltage to operate, and operation in that mode decreased in duration as the flow rate decreased. For the ethylene tests, there did not appear to be any stable operating modes, but there was a high reduction in voltage for the 25.2 SLPM flow rate.

## III.C: Arc Gap/Voltage Gradient Characteristics

Knowledge of the voltage gradient as a function of plasma torch arc gap is useful information to have when planning for future plasma torch applications. A fundamental consideration is the effect that changing the arc gap and fuel type has on the required voltage. Different arc gaps may provide stable regimes in which the torch prefers to operate, extending operation time and electrode life. In general, observing how the plasma torch operates under different conditions yields a better understanding of how it works.

### Test Procedure

In order to minimize the number of variables, only the arc gap and fuel types were changed. Every test was run at 30 SLPM (or about 1.72-2.07Mpa in the gas line), on either methane or ethylene, and at constant DC current. Initially the plasma torch was set to its normal 0.178mm arc gap and run at approximately 25A. The plasma torch was started on high frequency current and then allowed to run on DC only. Once DC operation was initiated, the data acquisition system was turned on. The plasma torch was run for 15 sec and then allowed to cool down. The arc gap was then adjusted to a higher value, and the test was repeated. This procedure was repeated until the arc gap was too large to allow torch operation on pure DC. The voltage data for each fifteen second test was then averaged to produce a single data point. A first-order, least-squares curve fit was then applied to the data to produce a smooth function of arc gap versus voltage. A first-order curve fit was used because it was found that under a pressure of about 0.811Mpa, voltage gradient versus arc gap for most gases is linear [28].

### Results and Discussion

The curve fits for the arc gaps vs. voltage tests are shown in Fig. III.C.1. It is apparent that ethylene has a much higher voltage gradient (≈180 V/mm) than methane (≈35 V/mm).

Typically it is easier to crack, or break the chemical bonds, of a more complex hydrocarbon, and

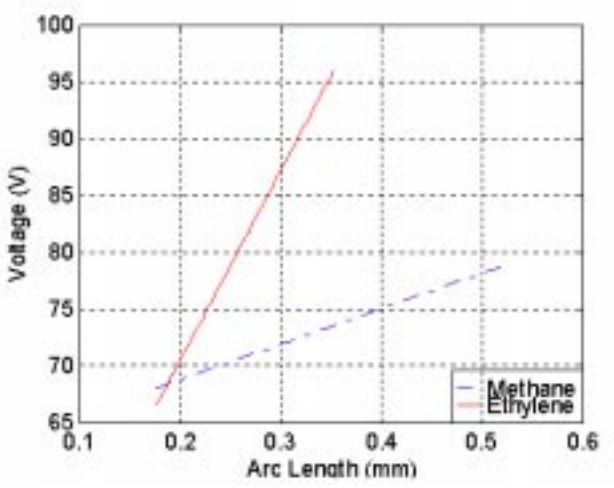


**Figure III.C.1: Arc Gap Influence on Voltage**

therefore should not require as much work as a simple, stable hydrocarbon. However, since there is an increase in density with more complex hydrocarbons, there is more resistance between the electrodes and in turn an increase in the voltage required to attach an arc.

Above an arc gap of 0.35mm, ethylene required too much power from the power supplies to run on DC current only. Methane reached this limit at about 0.52mm. Obviously, methane has a much wider band of operation and is more tolerant to arc gap settings than ethylene.

Although arc gap plays a significant role in determining the required voltage to produce

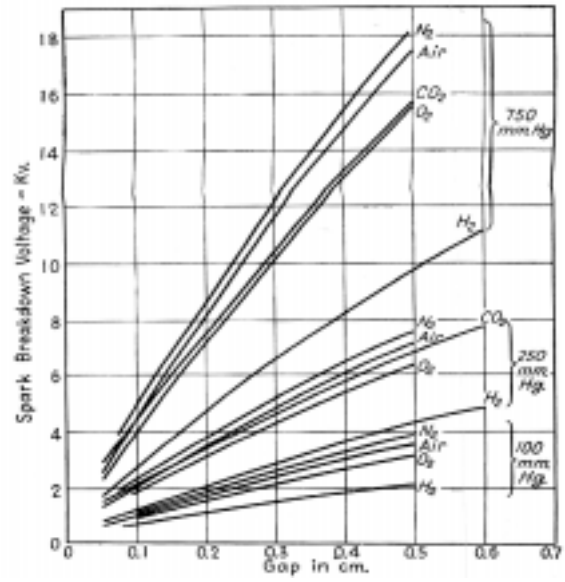


**Figure III.C.2: Breakdown Voltages for Various Gases from [15]**

an arc, pressure is also an important consideration. Figure III.C.2, a graph of spark breakdown voltage for equal sphere electrodes, shows that, for some common gases, as pressure increases so does the voltage requirement [29].

Therefore, as far as flow rate conditions are concerned, it would be ideal to discover the minimum required flow rate for a particular application to keep power requirements down.

Arc gap also has an influence on stability of the arc. In Figure III.C.3, the torch operational power is plotted as a function of increasing arc gap. Initially the required power

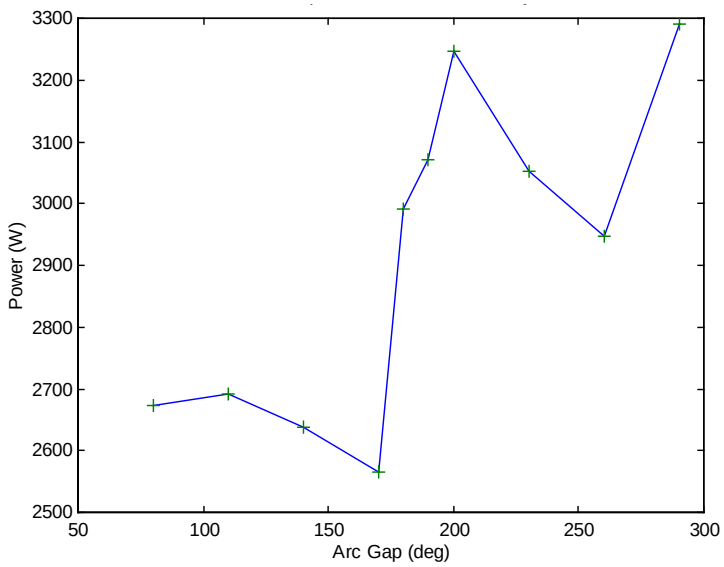


**Figure III.C.3: Arc Gap Influence on Arc Stability with Methane**

increases slightly, then drops nearly 150 W over the next 70° (0.125mm). There is a rapid increase in power over the next 30° (0.053mm) gap increase. This may be a result of transition between operating modes as seen with the voltage/current characteristics. Again, the operating mode idea is supported by a decrease in power over the next 70° gap increase. Finally, the last jump in power became to great, and the torch would not operate beyond this gap length.

## Final Remarks

The arc gap versus voltage gradient tests concluded that ethylene produces a much higher voltage gradient than methane. This reduces the amount of flexibility (range of arc gaps and voltage) with which the plasma torch can operate when operating on ethylene. Higher voltage also increases the electrode erosion rate and reduces the operating life of the plasma torch. However, it may be possible to determine an arc gap at which ethylene would operate in a low power mode, thereby extending the electrode life.

## III.D:Analysis of Plasma Torch Coking

Reliability of a plasma torch igniter in a supersonic combustion environment is of primary interest. Failure could result in loss of engine efficiency or even total engine failure, which in turn will result in mission failure. Heavy levels of coking (carbon buildup or soot) can plug the anode orifice, which makes it impossible for the plasma torch to operate effectively. Emissions of carbon-based particulate matter in diffusion flames can result from either rich operation or fuel additives.

Soot has long been recognized as a major pollutant. Regulations have been imposed to control soot emissions from various combustion devices including gas turbines. Also, soot particles can substantially increase the radiant heat transfer to engine components. Designs must be capable of withstanding higher temperatures depending on the amount of soot produced [30]. Particulate matter also poses a problem of clogging engine components such as injectors, or in the case of a plasma torch, the anode orifice.

In order to control the level of soot production, one must understand the chemistry behind soot formation. The first step of soot formation is nucleation. Nucleation occurs when fuel molecules dissociate into smaller hydrocarbon radicals upon heating. They then polymerize into much larger chains and soot precursors. The second step is the growth stage. This stage is characterized by the major bulk of soot production. Gas phase hydrocarbons condense onto the soot precursor molecules forming nearly spherical particles. During the oxidation phase, these particles are burned and form the carbon deposits we recognize as soot. Soot production is dependent on the rate of reaction of all three stages [30]. In the case of a plasma torch, nucleation of the fuel would occur from the fuel interaction with the arc. Polymerization and the growth stage should occur normally, but “burning” of the soot precursors couldn’t occur until the plasma stream interacted with air. Therefore, any soot that was deposited on the inside of the plasma torch would either indicate that air was present or that the soot was of a different chemical blueprint than what one would usually characterize as soot. Soot production is also dependent on the amount of several radicals, which may be present during combustion. Radicals can increase or decrease the sooting tendency of diffusion flames depending on which radicals are formed. Naturally, radical production is a function of the fuel being used, method of

combustion and fuel-air ratio. As an example, the presence of OH and O radicals can significantly increase the formation of soot [31]. However, without the presence of oxygen in the hydrocarbon feedstocks, these radicals couldn't be produced. The chemistry of soot formation in diffusion flames is well defined, but soot formed from hydrocarbon-arc interaction is not as well understood [27].

## Test Setup and Procedure

Plasma torch tests were conducted using argon, methane, ethylene and propylene. Both methane and ethylene were industrial grade, 99.8% pure. (An important fact in order to rule out fuel additives as a cause for coking) The propylene was 99.0% grade which is slightly lower than the other hydrocarbon fuels, but still quite pure. After a particular test series was finished, the Virginia Tech plasma torch was disassembled and simple inspections of the anode and cathode were made to determine whether or not coking occurred. After each test, the electrodes were cleaned using acetone to determine whether a blackened electrode was covered with soot or just discolored from the high temperatures present in the plasma torch. Before the HF starter was implemented into the lab setup, tests run using ethylene experienced a much higher level of soot production than did tests run using methane. It was found that, after the implementation of an external high frequency starter box, all coking problems disappeared completely. All tests conducted using this device were run with frequency settings of 5% or below.

## Results and Discussion

While using the four Miller welding units' high frequency starters to conduct tests, several conditions were present which affected whether or not coking occurred. In many of the tests, a flame plume was produced downstream of the plasma jet. On several occasions, the arc would be so unstable that it would blow out and allow the flame plume to enter the torch. A quick flame burst then forced itself through the anode seal and out between the anode cap and

torch body. After each one of these tests, heavy coking was present. Figure III.D.1 shows a comparison between the downstream side of an anode with heavy coking (left) and an unused anode (right). The upstream sides of the anodes show similar characteristics.

**Figure III.D.1: Plasma Torch Anodes**

Another condition that aided in the production of soot was the intensity of the high frequency that the Miller welding units supplied. With an open circuit voltage of 270 V, very little AC signal was needed in order to ignite the plasma torch. The high frequency starter on the Miller welding units greatly exceeded this need. The tests that did not experience some sort of flame burst, failed due to a soot plug that formed in the upstream side of the anode throat. This mode of failure developed over the course of a few minutes as the soot plug slowly formed. Formation of the soot plug was thought to be related to the amount of high frequency present. Throughout the entire test series, the torch was run under many different conditions. Variations in current, torch pressure and feedstock flowrate did not have as noticeable an effect on the production of soot as the use of high frequency current did. It is possible that the amount of high frequency signal used in running the torch may affect the rate at which soot is formed. (i.e. more HF increases nucleation-growth-oxidation reaction rate)

The use of a Miller HF-251D-1 high frequency starter box alleviated all of the coking problems experienced during earlier tests. All tests run with the HF-251D-1 experienced no coking whatsoever. This was mainly due to the ability of the HF-251D-1 to operate with very small frequency intensity settings. Tests where the HF-251D-1 was used to ignite the torch, but then turned off to allow the torch to run on DC only showed similar results. Also, a bluish discoloration of the downstream anode surface was observed during most tests. The cathode showed no signs of discoloration. Clearly, the discoloration is an indication of the higher temperature reached by the tungsten anode and chemical interaction with the air on the outside surface of the plasma torch.

## Final Remarks

Strong evidence indicates that the use of a variable high frequency starter box, operating at very low intensity, can significantly decrease or, indeed, eliminate the amount of soot produced during plasma torch operation, as experienced with the Miller HF-251D-1 used in conjunction with the Virginia Tech plasma torch. Coking is dependent on the amount of high frequency present, fuel to air ratios, fuel additives and the type of hydrocarbon feedstock being used. Important considerations must be made when choosing feedstocks and test conditions that a plasma torch will operate with. Coking can seriously impair the ability of a plasma torch to operate by plugging the anode orifice. The amount of high frequency used was determined to be the main cause of soot formation in the plasma torch, since fuel additives were present in only minute amounts and there was no air in the plasma torch interior where some of the coking occurred. Although the use of high frequency is needed only to ignite the torch, a small amount of high frequency is desirable in order to keep the electrodes cool and prevent excessive electrode wear. Future tests could be conducted to determine the amount of soot production for various levels of arc frequency in order to determine when soot production becomes a significant problem. This would provide an upper limit on frequency usage if high frequency current were to be used to sustain a plasma torch's operation time.

## III.E: Electrode Erosion

The original goal of the redesigned Virginia Tech plasma torch was to attain the ability to operate on pure argon for a period of at least twenty hours without failure [27]. Hydrocarbon fuels significantly reduce this operating time by eroding the plasma torch electrodes. Methods to extend electrode life must be found in order to have extended mission lifetimes, on the order of hours.

### Test Setup and Procedure

Five newly machined anodes and cathodes were used to conduct the electrode erosion tests. Each anode and cathode was labeled and grouped in pairs. Each electrode was weighed with a digital analytical balance before and after each test. The analytical balance had an accuracy of ±0.001g. Each set, consisting of an anode and cathode, was used only once. The time each test took was recorded to calculate the erosion rate. The number of high frequency starts required to get the torch running was also recorded, since a significant amount of electrode loss occurs during startup. All tests were conducted using high frequency and operating in the high voltage mode. The original goal was to run each test for fifteen minutes and then shut off the power to end the test. The same flow rate, current and gap setting were used for each test. One test, using ethylene, was conducted without the use of a flow swirler to determine the true effectiveness of swirling the arc.

### Results and Discussion

Despite continued efforts, the plasma torch was unable to run on ethylene for more than approximately nine minutes due to the high rate of electrode erosion. A tungsten plug formed on the diverging section of the anode nozzle and ended the ethylene tests prematurely. Methane ran quite easily and was allowed to run up to twenty-six minutes before power was turned off. A tungsten plug was never formed while the plasma torch was operating with methane.

Overall, ethylene was found to cause a much higher rate of electrode erosion than did methane. The results of the five electrode erosion tests are shown in table III.E.1.

**Table III.E.1: Electrode Erosion Results**

| Feedstock | Run Time (min.sec) | Anode Erosion (mg) | Cathode Erosion (mg) | Total Erosion Rate (mg/min) |
|---|---|---|---|---|
| **Test #1 Ethylene (no flow swirler) 1 start** | 3.00 | 27 | 34 | 20 |
| **Test #2 Ethylene 3 starts** | 4.10 | 40 | 6 | 11 |
| **Test #3 Ethylene 1 start** | 8.40 | 11 | 1 | 1.4 |
| **Test #4 Methane 1 start** | 26.00 | 10 | 1 | 0.42 |
| **Test #5 Methane 1 start** | 26.00 | 2 | 2 | 0.15 |

It is clear that a plasma torch operating with ethylene, on average, would have a much shorter operating lifetime than a plasma torch operating with methane due to electrode erosion. These results uphold qualitative observations made throughout the entire testing series. A possible explanation for this phenomenon is that ethylene has a more complex chemical structure than methane, namely that ethylene has four single covalent bonds and one double covalent bond, while methane has only four single covalent bonds. Double covalent bonds have much higher bond energies than single covalent bonds. They would, therefore, require more power to break in order to ionize the molecule. Power levels for ethylene and methane both averaged about 2.2 kw, but power levels for ethylene generally had larger peaks. Another possible explanation why electrode erosion rates are higher for ethylene is because ethylene plasma might be more erosive on tungsten than methane plasma. Most of the anode mass loss occurred on the

upstream side of the anode constrictor where plasma was present. This suggests that anode erosion may be a function of both power level and the nature of the plasma.

A majority of electrode erosion was confined to the anode. Intuitively this is reasonable, since the arc passes from the cathode to the anode. Analogous to this type of arc characteristic would be pouring water into a glass. While the stream of water (arc path) is smooth and laminar from the spout of the pitcher (cathode), it produces violent disruptions in the glass when it strikes the bottom (anode). The opposite would be true if the polarity were reversed and current passed from the anode to cathode. Combining the effects of arc characteristics and the nature of the plasma produced provides a clearer picture to why electrode erosion occurs and how to minimize it.

The use of a flow swirler reduced the amount of cathode erosion by as much as 700%. Anodes did not experience this amount of reduction, but did see some improvement. Reduction in electrode erosion using a flow swirler could not be truly quantified, because the number of new cathodes and anodes available limited the small number of electrode erosion tests. However, it is still quite evident that swirling the flow does improve plasma torch performance, by producing steady operation, and lengthens the lives of the electrodes.

Throughout the entire testing series, it was observed that a large amount of electrode emission occurred during initial startup. Electrode emission is characterized by yellow streaks of light emanating from the plasma torch nozzle, caused by the hot metallic particles leaving the electrodes with the flow. These particles are hot enough to initiate a reaction with the oxygen in the air, resulting the yellowish glow. A picture of electrode emission during startup is shown in Fig. III.E.1.

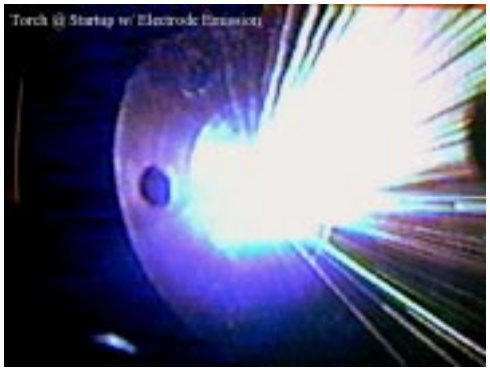

**Figure III.E.1: Torch Startup with Electrode Emission**

Once the torch was operating under steady conditions, electrode erosion diminished significantly. One of the tests conducted using ethylene, test #2, required three starts in order to get the torch operating. This test experienced four times the amount of electrode loss as did the ethylene test requiring only one start, test #3, and ran for roughly one-half of the time. Therefore, it can be concluded that a significant portion of electrode loss occurs during startup.

## Final Remarks

The electrode erosion tests yielded several important results that must be considered when operating a torch with hydrocarbon fuels. First, hydrocarbon feedstocks, in general, will significantly reduce the life of an electrode due to the high rate of electrode loss when compared to operation with argon or nitrogen. Between the two hydrocarbon gases tested, ethylene produced a much higher rate of erosion, on average exceeding that of methane by about 400%. During most of the tests, the anode experienced considerably more mass loss than the cathode, particularly when the plasma torch was operating with ethylene. Also, the use of a flow swirler to induce rotation in the arc significantly increases the life of an electrode, regardless of the gas being used. The electrode life is of utmost importance when considering the purpose and mission time of the plasma torch. Purely from an electrode-life analysis, methane is a more suitable plasma torch feedstock than ethylene.

## III.F:Plasma Torch Start/Restart Capabilities

In scramjet missions, the ability to start and restart the engine is of considerable importance. Rapid shutdown and delayed re-light may be necessary to meet a changing mission profile. In addition, extreme turbulence or inlet flow distortion could result in engine flameout requiring multiple restarts. With these needs, it is important to develop a highly reliable plasma igniter for use in scramjet engines.

In order to meet the demand for high reliability, the Virginia Tech plasma torch had to demonstrate the ability to start and restart in various operating situations. Since variables such as mass flow rate, torch chamber pressure, current setting and high frequency intensity may affect the ability of the torch to operate, variation in each should be investigated. Due to the ease in which the mass flow rate could be controlled with the Sierra 840M units, variation in mass flow was chosen as the starting point for the testing.

### Test Setup and Procedure

A standard equipment setup was used for this series of tests with the following modification: due to the use of a high frequency signal, the data acquisition system was disconnected from the power supply circuit. The power supplies were each set at approximately 15A, and the HF starter was set at 5%.

The same testing procedure was used in the analysis of both methane and ethylene. Starting at a specific flow rate, each of the four power supplies was turned on. The HF starter was powered up, and, following a brief pause, the continuous mode switch was activated. The torch was run for one minute with the HF starter operating the entire time. At the end of the minute, the HF starter and power supplies (if necessary) were turned off for five seconds, to simulate a flameout, then restarted. The torch was run for a period of 15-20 seconds after restart was established, at which point the HF starter and power supplies were again shut off.

After a short cool-down period, the flow rate was increased by 2 standard liters per minute (SLPM), and the above procedure was repeated. In all, sixteen tests were completed (8 methane and 8 ethylene) from a range of 16 SLPM to 30 SLPM over a period of two days.

## Results and Discussion

Test results were determined to be highly successful since the torch was able to re-light on the first attempt for all 16 test runs. During low flow rate tests, the torch operated with intermittent fluctuations, but was mostly steady throughout the first 40-50 seconds of the test. At nearly one minute of ethylene operation with flow rates near 16 SLPM, fluctuations in the plasma jet were quite severe. However, upon restart, the plasma jet reformed to a smooth operating mode similar to that of initial startup. Higher flow rates generated a smooth, stable jet devoid of fluctuations over the entire minute for both gasses. The high flow rates also had instant reformation of a steady jet on restart.

These observations indicated that flow rates near 30 SLPM were more favorable for operation at than low rates around 16 SLPM. Furthermore, restart of the torch established a steady plasma jet over the full range of flow rates. Also noteworthy, methane operated with less jet fluctuations than ethylene did, but the torch re-lit with the same ease operating on both gases.

## Final Remarks

Due to the importance placed upon reliability of the plasma torch, the results of the start/restart tests are quite significant. With the high success rate of the plasma torch on restart, a minimum of redundancies would have to be included in any engine configuration. With fewer redundancies, lower weight and, in turn, lower cost could be achieved at initial manufacture. Over the life of engine production, the savings could amount to a significant sum.

Although the 15A and 5 % HF setup had perfect restart performance over the described flow rate range, more testing should be done for higher and lower current levels in order to

obtain more verification that the plasma torch will “always” restart. Also, starting at various current settings will simulate starting and restarting in off-peak power situations that may occur in actual operation.

## III.G: Torch Body Temperature Tests

The temperature of engine components can have important effects on multiple engine systems. Since heat from the torch will conduct to other engine components and the main gas flow, there may be a need for modifications to the cooling system. Also, a hot spot on the engine wall may adversely affect the flow properties resulting in loss of engine efficiency. In an effort to control this localized heating, tests were conducted to determine the transitional and steady state torch body temperature.

### Test Setup and Procedure

A methane flow rate of 30 SLPM or 20 SLPM for argon was set. A current setting of 27% (about 40 A) was primarily used, except for one run with argon. With the flow rate and current set, the torch was started with the HF starter. The DAQ system was simultaneously started with the torch, which allowed temperature data to be received from the type K thermocouple located on the torch body. The tests were run until a constant temperature reading was reached, or when the torch flamed out.

### Results and Discussion

Test results indicated higher current settings, lower flow rates and less complex gases yielded higher body temperatures. As seen in Figure III.G.1, the highest body temperature was reached with argon (790K or 970°F). There was a dramatic reduction in maximum temperature for argon when the current setting was reduced to 14%. Obviously this was an effect of adding less energy to the system.

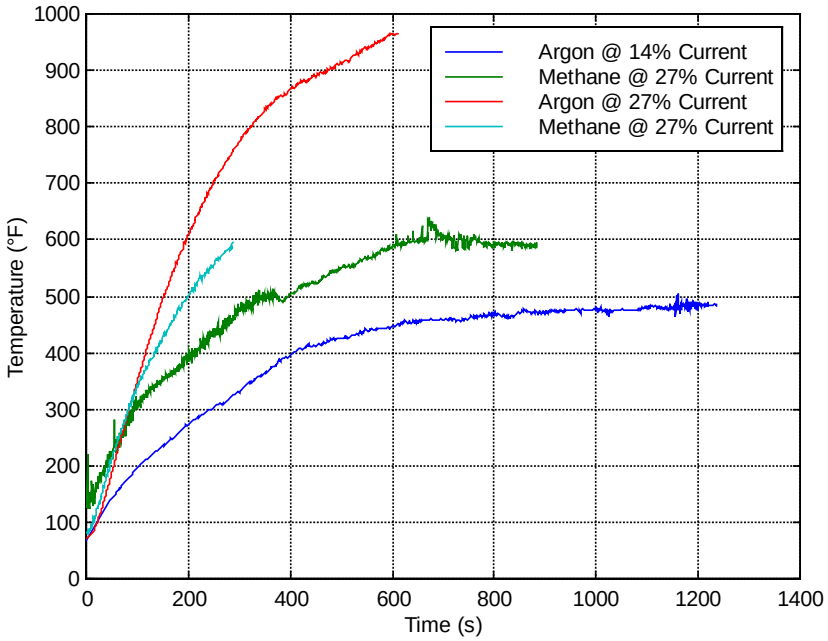


**Figure III.G.1: Torch Body Temperature vs. Time**

The two methane cases were run at the same current setting, but the lower temperature case, as indicated by the green line, was run at 20 SLPM instead if 30 SLPM. The 20 SLPM case did not run for a long time, but the data taken does show that the slope of the transitional portion of the temperature curve is higher than the 30 SLPM case. This would make sense, since the higher flow rate is able to carry away more heat than the lower flow rate.

Of the four cases, two were run at exactly the same conditions, but with different gases. Of these cases, methane had a lower overall temperature than argon. One reason for this is that more energy goes to breaking down the bonds of the $CH_4$ (methane) into carbon and hydrogen, then ionization, whereas a majority of the electrical energy is used to directly ionize the argon.

It should also be noted that although these four cases differ in some way, the maximum, or steady state, temperature occurred within 600 to 800 sec (about 10 to 12 minutes). This is important since some missions employing a plasma torch igniter may only take one minute, which correlates to 340-700K (150- 250° F), and a specific design could possibly ignore this small temperature increase.

## Final Remarks

These tests were successful in determining factors such as flow rate, current setting and gas type that affect maximum torch body temperature. Intuitively, a high flow rate and low current setting would reduce temperature since there is more ambient temperature gas rapidly entering and less energy being put into the torch system. However, some knowledge of the molecular interactions and the energy needed to break those bonds is required to have a feel for the reduction in temperature as feedstock complexity increases. A combination of these factors can be used to control the transition and maximum temperature of the torch if necessary. Also, knowing what level of heat addition is coming from the torch can be important to the design of an engine cooling system.

## III.H: Propylene Operational Characteristics

In the effort to generate a stable plasma jet with liquid fuel such as JP8, small increases in the complexity of the gases being tested must be made. Initially, methane ($CH_4$) was tested, since it is the most simple hydrocarbon fuel. Following those tests, ethylene ($C_2H_4$) was experimented with to see how the extra carbon affected torch operation. Propylene ($C_3H_6$) was chosen as the next step in increased complexity since it has a C to H ratio (1:2) similar to ethylene. Data from this third fuel will be used to analyze how increased complexity affects the plasma arc and also will provide a broader database to which future analysis of liquid fuels, such as JP8, can be compared.

### Test Setup and Procedure

Testing with propylene focused on aspects such as operational feasibility, electrode erosion and power requirements. Operational feasibility, or attempting to light the torch, was simply a matter of choosing a flow rate (16.9 SLPM), setting the current (27%) and turning on the high frequency starter. Lower settings were then chosen in an effort to find lower limits of propylene operation.

Electrode erosion was tested in a similar manner as the methane erosion tests were done. New electrodes (2 cathodes and 2 anodes) were weighed and their mass was recorded. The current was set at 27% and the flow was set to 14.1 SLPM of propylene and 10 SLPM of argon. The torch was started and forced, by restart if necessary, to run for at least one minute. After the test, the electrodes were weighed again and the mass was recorded. The test was repeated with the other pair of new electrodes.

To see how much power was required to operate propylene, test runs were conducted at 27% current while the flow rate was varied. The test was run until the torch flamed out.

## Results and Discussion

Operation of the torch on propylene was achieved at the full 30 SLPM and 27% current, however, within about 10 seconds, there was a flameout in the back of the torch. The flow rate was reduced to 25 SLPM and ignition was re-attempted. Again, within a short time, a flame appeared in the back of the torch and shutdown had to be initiated. The current setting was reduced to 14% in order to generate a smaller plasma jet and plume. The reduced plume would be less likely to ignite any gas leaking from the back of the torch. The torch started with the HF starter, but went out when the power supply was returned to straight DC operation. Ignition was re-attempted several times, but the torch would not remain lit without the starter on.

The power supplies were returned to 27% current, but for the next attempt, 5 SLPM of argon was added to the 30 SLPM propylene flow. When this mixture was ignited, the torch flamed out within 20 seconds. For the next attempt, the argon flow rate was increased to 10 SLPM and the propylene flow rate remained the same. With these settings, the torch ran for nearly one minute.

During the feasibility tests, power data was continually being collected. As seen in Fig. III.H.1, at constant current setting and constant flow rate, there is a transition period before an

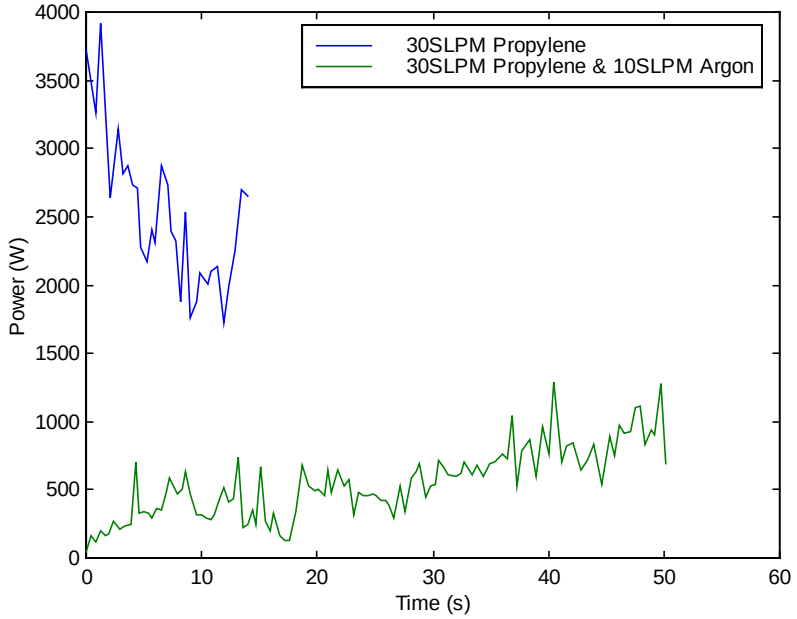


**Figure III.H.1: Torch Power (27% Current)**

equilibrium power level is reached. For pure propylene, this occurs in about 10 seconds and is at approximately 2000 w. When the argon carrier is introduced, the transition takes nearly 45 seconds, but the power reaches a maximum at about 950 w.

To better understand how the amount of argon affects the power required in a propylene flow, the flow rates of both gases was varied while the current setting was held at 27%. Figure III.H.2 indicates how power varies with different combinations of flow rates.

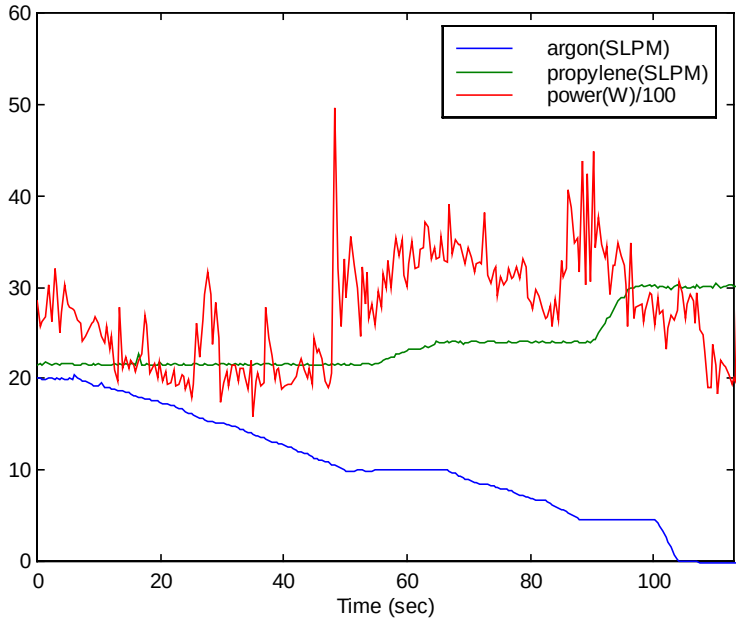


**Figure III.H.2: Propylene Power Tests**

The initial argon flow rate is 20 SLPM, and propylene is set to 22 SLPM. As the argon flow rate is reduced, there is a slight reduction in power until about 20 sec, where the power level remains constant on average. Around 50 sec, the argon flow is held constant at 10 SLPM while the propylene flow rate is gradually increased. During this increase, the slope of the power curve becomes greater and the power peaks at around 3800 w. At this point, further decreases in argon flow rate reduce the required power until about 5 SLPM of argon is reached. Near the end of the run, as propylene is set to 30 SLPM and the argon flow is stopped, the power level drops to near 2000 w, which is consistent with the results from the previous figure.

During these tests, there appeared to be large amounts of electrode emission. The results of the erosion tests, given in Table H.1, indicate significantly larger amounts of electrode erosion than methane or ethylene.

**Table III.H.1 - Electrode Erosion**

| Feedstock | Run Time (min) | Total Erosion Rate (mg/min) |
|---|---|---|
| Propylene 1 | 2.166 | 69.4 |
| Propylene 2 | 2.833 | 89.5 |
| Average Ethylene | 5.280 | 10.8 |
| Average Methane | 26.000 | 0.285 |

On average, the propylene erosion rate is 8 times as large as ethylene and 280 times that of methane. This trend of increased levels of electrode erosion with increased fuel complexity may be attributed to the greater power required to breakdown the carbon bonds. The increased power is a result of increased current, which is simply a greater flow of electrons between the electrodes.

## Final Remarks

In general it can be stated that increased complexity of the fuel makes torch operation more difficult, but operation can be achieved. Extended duration is possible with the introduction of a carrier gas such as argon. In addition, reduction in required power is a benefit from the argon carrier, however a separate gas system is undesirable due to added engine complexity and weight.

The large amount of electrode erosion is important in that it reduces component life, but the addition of heated particles to the flow may be found to enhance combustion. Overall, unless methods are found to reduce the level of propylene erosion, the torch will continue to experience limited run times on this gas.

## III.I: Audio/Visual Plasma Torch Analysis

Acquisition of data from sources other than simple voltage inputs can give a more comprehensive picture of why the torch is operating in a particular way. Tests such as audio analysis, high-speed CCD camera photos and 35mm camera photos can provide important information about torch operation and flow structure. For instance, a variation in torch audio frequency may indicate faulty power supplies or connections. Similarly, pictures of the plasma jet may reveal a misdirected jet caused by a blockage in the flow path. In either case, problems such as these would not necessarily be discovered with standard temperature, pressure and power data.

### Test Setup and Procedure

The audio tests required the use of a BNK microphone connected to a portable National Instruments data acquisition system. The DAQ output was fed into a laptop computer using LabView software. A flow rate of 20 SLPM was set and the power supplies were set to 27% current. Before the HF starter was activated, the background noise signature was recorded. The torch was then started and allowed to run for about 10 seconds before the audio system recorded the torch operation.

Both argon and methane were used in the high-speed photo tests. These tests, which used an EG&G Reticon digital camera with zoom lens, were timed so that startup and the first 1.5 seconds of operation were recorded. This camera was capable of taking up to 1000 frames per second of black and white pictures for up to 2 sec. Initially the methane flow rate was set at 25 SLPM and the power supplies were at 27% current. The DAQ system was started and approximately 0.5 seconds afterwards, the torch was started. After a couple seconds the torch was shut off. This process was repeated at the same current setting, but reduced flow rates of 20, 15 and 10 SLPM. Similarly, tests with argon were conducted at 20, 15 and 10 SLPM also at the 27% current setting.

Two types of 35mm cameras were used to observe normal torch operation, a conventional film camera and a digital camera. The digital camera was on hand throughout all the test series and on occasion, a few pictures would be taken and analyzed. As a result of always having the camera, pictures were taken of argon, methane, ethylene and propylene. The film camera was a Minolta with zoom lens and a roll of film was taken during a methane test dedicated to optical examination.

## Results and Discussion

The results of the audio spectrum analysis, Fig. III.I.1, indicate a distinct peak at 180 Hz. This peak, which is not present in the background noise, is complemented by a higher harmonic

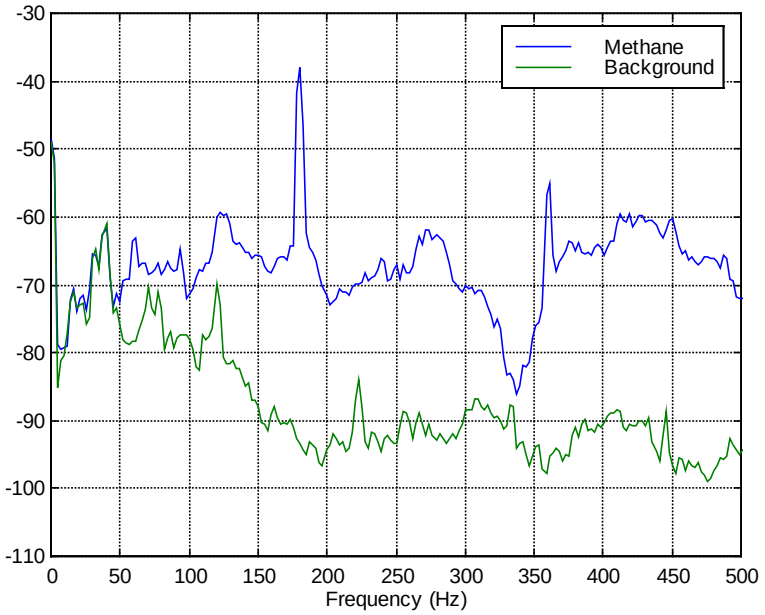


**Figure III.I.1: Acoustic Test of Methane Operation**

at 360 Hz. Initially, the cause of this peak was unclear, however, upon further investigation, it was found that the power supplies operated at this same frequency. This knowledge is important since it is possible to control torch frequency with the power supply. Also, it is noted that there

are no intense audio signals at other frequencies, so controlling this signature is more easily accomplished than controlling a complex signal with multiple peaks.

Pictures taken with the high-speed CCD camera were essential for analysis of the initial formation of the plasma jet and plume. These photos, each capturing one millisecond of torch operation, were used to identify plasma and flow characteristics impossible to see with the naked eye. Figure III.I.2 contains a series of torch startup pictures capturing the first 9ms of operation using argon. The frame sequence begins with the upper left image and proceeds to the right, as if

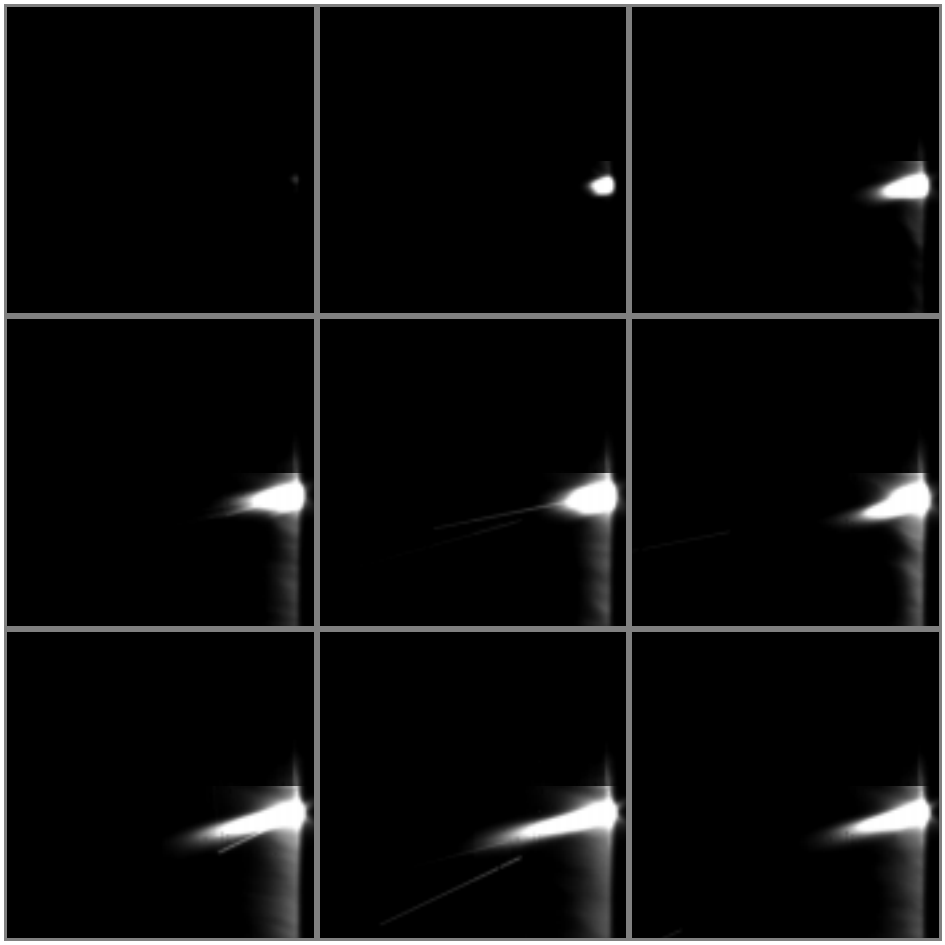

**Figure III.I.2: Torch Startup with Argon (1 ms between frames)**

reading a book, with the lower right image being the closing frame. Note that the viewing area is 150% actual size and the photos are in black and white. By frame three, it is clear that the plasma jet is pointing slightly downward which may be caused by a partially blocked or non-symmetric anode. Frames 5, 7 and 8 capture electrode emission from the torch, however this is

quite a small amount compared to operation on other gases. There appears to be a large strip of ionized gas heading downward below the plasma jet, which is most likely a reflection off the anode face caused by the camera angle. The jet becomes largest in frame 8 but this is still only approximately 1.1 cm.

Unlike the argon flow, methane starts with a larger, more energetic plume that is also pointing slightly downward (Fig. III.I.3). Again the vertical spike can be seen near the anode exit, which is thought to be a reflection. In frame 5, the jet is beyond the edge of the viewing

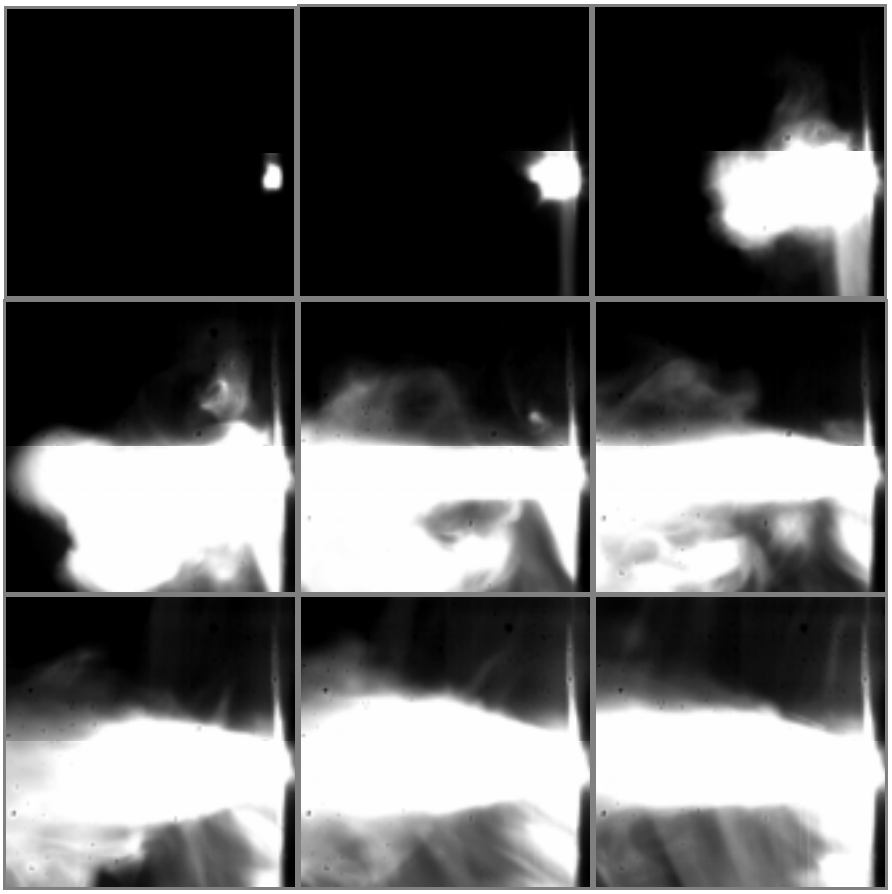

**Figure III.I.3: Torch Startup with Methane (1 ms between frames)**

area, therefore its size cannot be accurately measured. Also in frame 5, the beginning of a circulating portion of the jet can be seen. In the following frame, this circulated portion of ionized gas is nearly isolated from the main flow. It is important for combustion purposes to see that "pieces" of hot plasma can sustain themselves within the flow, away from the main jet, to

possibly enhance fuel ignition. In conjunction with isolated plasma, the lighter shades of gray in the frames are actually flames generated from fuel combustion. These flames appear dark due to the requirement of very intense light to stimulate the CCD array in this particular camera setup. In any event, these flames are also quite important to aid in combustion of the fuel.

After startup, the CCD camera captured the torch operating for a short time. In one particular methane run, the swirl of the flow was actually clearly defined. Figure III.I.4 depicts

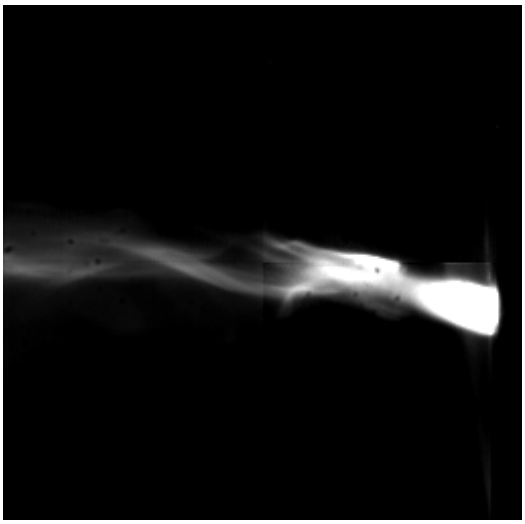

**Figure III.I.4: Flow Swirl with Methane**

the flow rotation along with another isolated plasma piece. The jet is upward pointing in this run, yet, unlike the startup pictures, there is a small plasma jet and large flame. There is a reason for the plasma/flame structure that is shown here. As seen with the audio signature, the torch power supplies oscillate at 180 Hz, therefore the plasma jet elongates and shrinks with this same frequency. More specifically, the growth/reduction process occurs at about every 11 frames. Therefore, in Fig. III.I.4, the plasma jet is on the shrinking side of this oscillation, and the residual flame is present due to the larger plasma jet that just receded.

It is not necessary to just record high-speed pictures of the torch operation to acquire useful information. As seen in the digital picture of the torch operating on methane (Fig. III.I.5),

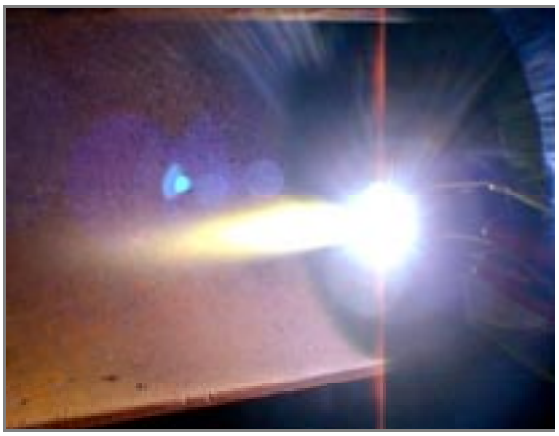

**Figure III.I.5: Temperature Strata in a Methane Plume**

there is a gradual color change from bright white to reddish-yellow as the distance from the center of the plasma jet is increased. These color bands define different temperatures of the combustion products and indicate that the sides of the plume near the anode have the highest temperature gradient.

Another useful low-speed image is Figure III.I.6. In this 35mm camera photo, a bright

**Figure III.I.6: Leak with Flame in Torch**

yellow flame can be seen during torch operation. When this happened the torch had to be shut down for safety reasons. Upon closer inspection, the top edge of the torch and the cathode adjustment piece can be seen in front of the yellow flame. That information, combined with the forward flowing direction of the flame, indicates that the flame is originating in the back of the

torch, possibly from a gas leak in the cathode adjustment piece. Also, the bright yellow color of the flame implies an oxygen rich flame possibly meaning that the leak is small, but enough to cause a problem. The usefulness of these pictures is apparent in that the location of leaks can be found without allowing the flame to persist long enough to visually inspect the torch, opening up the possibility that a fuel line could be breached.

## Final Remarks

From the data and images that were taken, it is obvious that alternative forms of data are very useful to help understand how the torch operates. The audio data can be used to help reduce engine noise and vibration, since the 180 Hz frequency may be actively or passively canceled. Also, an onboard microphone can monitor the operational frequency of the torch and any variation can be sent to the warning system, thereby reducing risk of engine out.

The high-speed images are essential for designers to improve plasma and flame flow from the anode, and to insure that components like the flow swirler are working properly. Similarly, low speed pictures can be used to improve torch operation. The temperature strata images can be used to determine the best injector orientation to insure that the hottest part of the plasma/flame is complimenting the fuel injection scheme. Also, fire location and, therefore, fuel leak location can be determined more safely with pictures.

# IV. Atomic Emission Spectroscopy

Analysis of the spectrum produced by the Virginia Tech plasma torch consisted of a series of experiments designed to collect spectral data while using methane, ethylene and propylene as feedstocks. These tests covered a broad range of wavelengths in an effort to identify any atomic or molecular species that were present in the plasma. Multiple tests were conducted for each gas to verify particular peaks and to prove repeatability of the data. In addition to coarse scans, focussed scans were conducted to search for hydrogen atoms at known wavelengths.

## Test Setup and Procedure

The variation on the standard equipment setup was the removal of voltage and current inputs to the computer to avoid an electrical surge when the high frequency starter was activated. In place of the current input, the two sides of the resistor across the PMT output were run into the ±50 mV signal conditioning module.

The test procedure started with setting the feedstock flow rate so as to maintain a chamber pressure of about 207 KPa (30 psia). This setting varied, depending on the gas being run through the torch and the condition of the electrodes. The current setting on the power supplies was set to the lowest setting that would allow stable operation for the longest period of time; again this varied with fuel type and electrode condition. With the flow rate and current set, the torch was started with the HF starter. When the torch ignited, the HF starter was turned off. Following HF shutoff, the spectrometer grating rotation motor and DAQ system were started simultaneously. Coarse scanning was completed at a rate of 500 Å/min from 3000 Å to 7000 Å, unless the torch extinguished itself. If the test lasted until the spectrometer wavelength counter reached 7000 Å, the torch was shut off, since both PMT and grating resolution dropped off at this point. After the test, the torch was removed from the test stand and inspected for electrode wear and damage. Once the torch was reassembled, the test was repeated to verify peaks.

Seventeen test runs were conducted: eleven runs using methane, four runs using ethylene and two for propylene. The first four methane runs were broadband scans ranging from 3000 Å

to 7300 Å, with a flow rate of 24 SLPM and current setting of 20%. Four ethylene runs followed, covering the same wavelength range, but at a flow rate of 36 SLPM and 20% current setting. At a later date, three more methane tests were run at 30 SLPM and 27% current to determine if there was any effect on the species produced by the torch. A similar study was conducted using a solid propellant pulsed plasma thruster [32], which found that the species formed did not vary with increased energy input. The tests looking for hydrogen atoms were conducted using methane at 20 SLPM, 27% current and a scan speed of 50Å/min. Lastly, propylene-argon scans were attempted, however, due to limited run times, minimal data was collected for this fuel.

## Results and Discussion

The output from the PMT for the first four methane tests is given in Fig. IV.1. Only the first two runs lasted the entire 4000 Å test range, however there was little concern since there were no major peaks beyond 5000 Å. The strongest peak occurred at 3854.3 Å and was confirmed by all four runs. According to a listing of typical flame emission spectra, the strong peak could be $C_2$ (3852.2 Å), CN (3854.7 Å) or $CO_2^+$ [33, 34]. In order for CN or $CO_2^+$ to form, the methane had to first be broken down into some partial carbon ion while flowing through the arc, then rapidly react with $N_2$ or $O_2$ in the air. In any event, both $C_2$ and CN are free radicals associated with combustion.

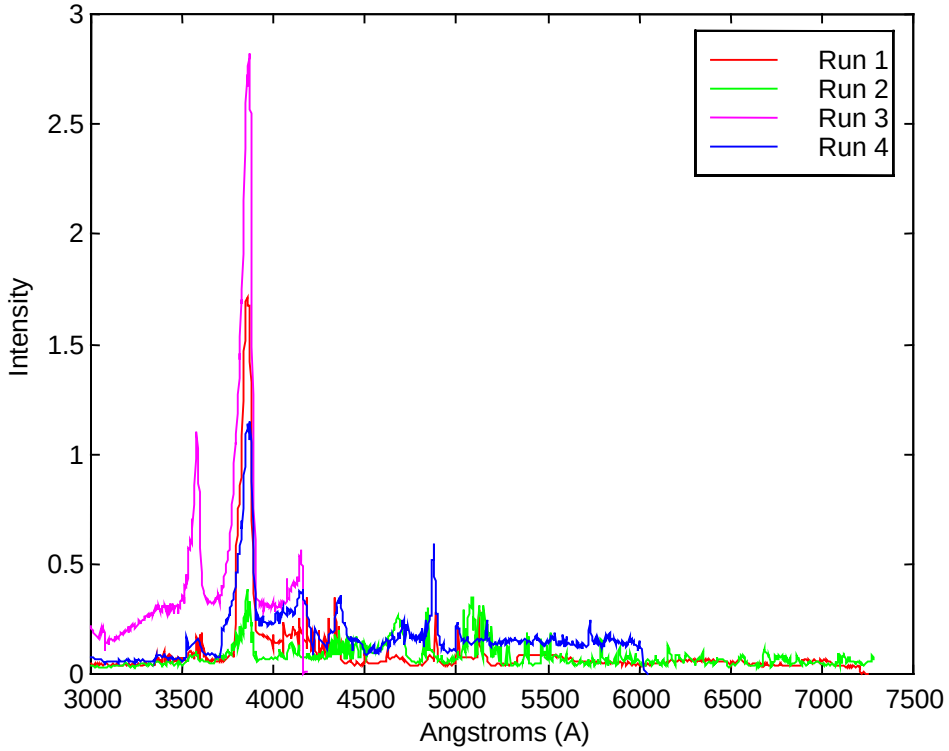


**Figure IV.1: Spectrograph for Methane at 24 SLPM and 27% Current**

Another strong peak was observed at 3577 Å. The closest molecular spectra to that peak would be $N_2$ at 3576.9 Å. A listing of other possible molecules present in the methane plasma are found in Table IV.1.

**Table IV.1: Species Present for Methane at 24 SLPM**

| **Peak (Å)** | **Possible Species Present – Wavelength (Å)** | | | |
|---|---|---|---|---|
| 4335 | $CO_2$ - 4335 | OH – 4336.6 | | |
| 4367 | $C_2$ – 4368.8 | $C_2$ – 4365.2 | | |
| 4679 | $O_2^+$ - 4678.5 | $C_2$ – 4680.2 | | |
| 4870 - 4880 | $H_2$ - 4873 | $O_2^+$ - 4877.6 | $CO^+$ - 4879.5 | $O_2$ - 4880 |

The data from the ethylene tests, Fig. IV.2, is less clear, but a well-defined peak occurs again near 3577 Å. As with methane, this peak could be $N_2$. Since the variation in the four runs is larger for ethylene, it is harder to determine exactly where peaks occur. However, if one assumes that each peak on a specific run is valid, then there are a large number of peaks in the ethylene graph. This is not too much of an assumption since it is known that each time an arc is formed, the composition of combustion products can vary [14].

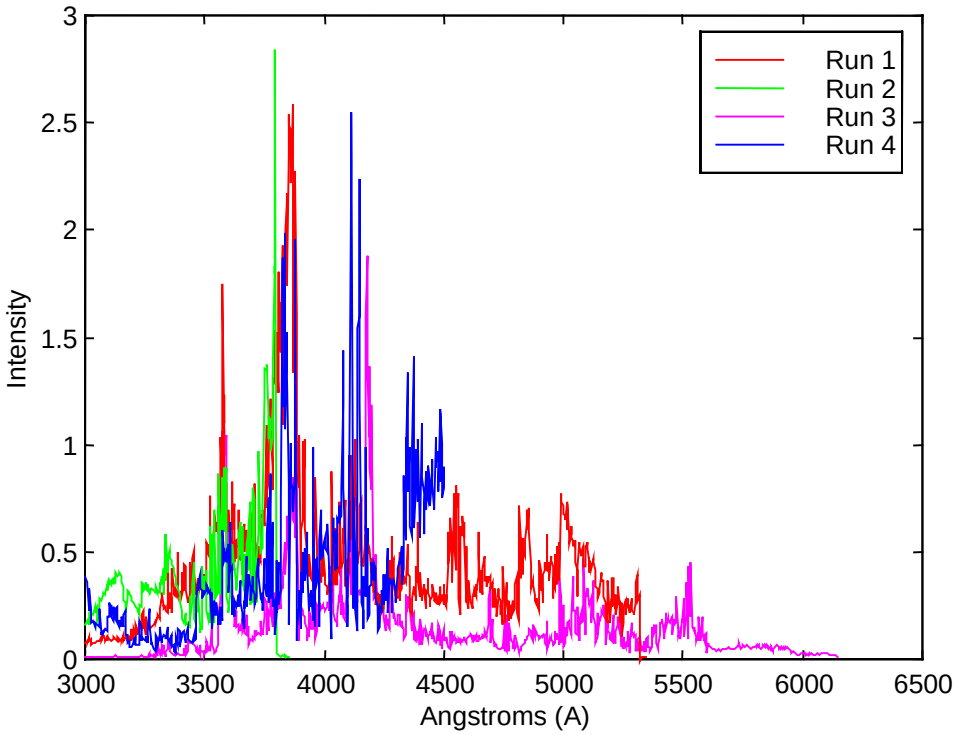


**Figure IV.2: Spectrograph for Ethylene at 36 SLPM and 27% Current**

The prominent peaks In Fig. IV.2 are organized in Table IV.2 in order of increasing wavelength. It should be noted that there were other products that had values near the peaks, but were outside the ±2 Å tolerance. Also, there were peaks at 4148 Å and 4691 Å where no species could be identified.

**Table IV.2: Species Present for Ethylene**

| **Peak (Å)** | **Possible Species Present – Wavelength (Å)** | | | |
|---|---|---|---|---|
| 3796 | $CO^+$ - 3795.8 | NH – 3795 | | |
| 3860 | $O_2^+$ - 3859.5 | $N_2$ – 3857.9 | $N_2^+$ - 3857.9 | CN – 3861.9 |
| 3955 | $CH^+$ - 3954.4 | $CO^+$ - 3953.6 | | |
| 4115 | $O_2^+$ - 4115.8 | $O_2$ – 4114 | | |
| 4179 | $O_2$ - 4179 | $CH^+$ - 4178.4 | $H_2$ – 4177.1 | CN – 4181 |
| 5084 | $H_2$ – 5084.8 | | | |
| 5533.5 | OH – 5534.1 | CO – 5532.5 | | |

When the current and methane flow rate were increased, there was not much difference in the shape of the PMT output curve (Fig. IV.3). Even though there was little difference in the

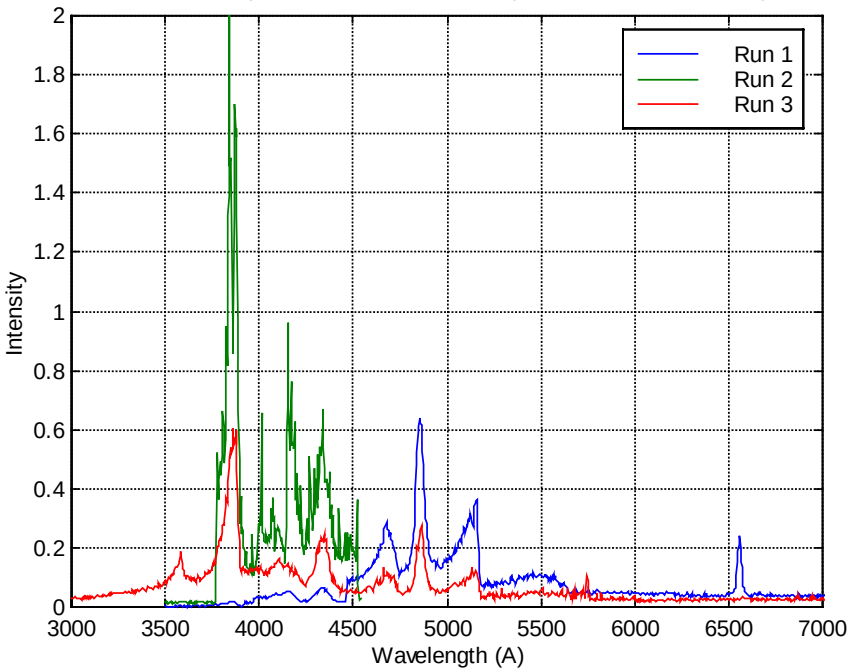


**Figure IV.3: Methane Spectrographs for 30 SLPM and 27% Current**

apparent shape, there was a slight shift in the values and intensities of the peaks. Upon investigation of these values, a distinctly different set of species was found. Table IV.3 lists the species most likely present with those at the left side of the table having the highest probability.

**Table IV.3: Species Present for Methane at 30 SLPM**

| **Peak (Å)** | **Possible Species Present - Wavelength (Å)** | | | |
|---|---|---|---|---|
| 3841 | $O_2$ - 3841 | $O_2$ - 3840 | $N^+$ - 3842.2 | $CO_2^+$ - 3838.8 |
| 4337 | OH - 4336.6 | WO - 4338.3 | | |
| 4679 | W - 4679.04 | C - 4678.6 | $O_2^+$ - 4678.5 | $C_2$ - 4680.2 |
| 4854-4862 | W - 4854.09 | $H_2$ - 4856.55 | $H_\beta$ - 4861.33 | W - 4863.08 |
| 5157 | CN - 5156.0 | | | |

Both sets of data have the 4679 Å peak; also the 4335 Å peak is close to the 4337 Å peak. Similarly, both data sets have a range of peaks in the upper 4800 Å wavelengths. The

comparability of both sets of data indicates that more tests should be completed to determine if correlation exists or not.

There are some small peaks that may be noise, however upon comparison of both sets of data there is enough repeatability to suggest a peak. One occurrence of this is at the 5575 Å wavelength, where only Run 4 of the 24 SLPM set and Run 3 of the 30 SLPM set have a peak. This could be the tungsten line at 5576.3 Å or $N_2$ at 5574.8 Å. Also, in Run 3 of the 30 SLPM set there is a peak near 3577 Å which is seen in all four 24 SLPM runs. This may be excited air at 3577.2 Å, $N_2$ at 3576.9 (also occurring in ethylene) or tungsten at 3576.7 Å.

The propylene tests continually flamed out until a significant amount of argon was mixed into the flow. Even with a carrier gas there were short run times, on the order of six minutes. Nonetheless, the results of two runs conducted at 500 Å/min are given in Figure IV.4. There is little correlation between the peaks of both curves throughout the test, except near 3102 Å. An

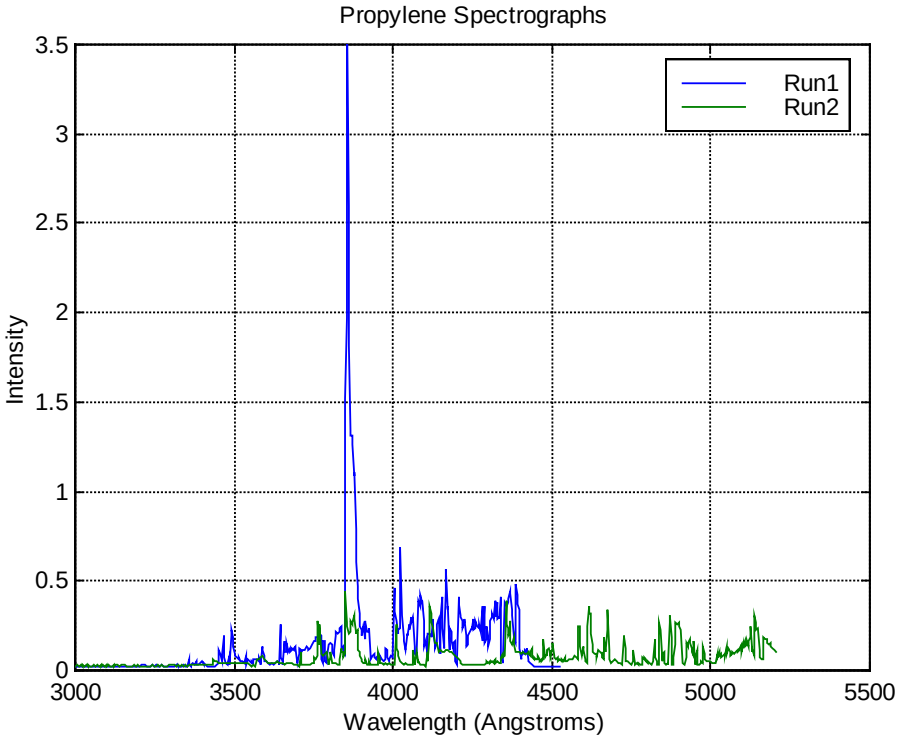


**Figure IV.4: Propylene Spectrograph**

attempt to identify all the peaks was conducted regardless, since repeated peaks may be found with further testing. A listing of possible species is given in Table IV.4 as was done for methane and ethylene.

**Table IV.4: Species Present for Propylene**

| Peak (Å) | Possible Species Present - Wavelength (Å) | |
|---|---|---|
| 3763 | $O^+$ - 3762.51 | $N_2^+$ - 3761.6 |
| 3768 | W - 3768.46 | |
| 3858 | $N_2$ - 3857.9 | $O_2^+$ - 3859.5 |
| 4117 | $CO^+$ - 4117.3 | $O_2^+$ - 4115.8 |
| 4353 | $C_2$ - 4353.0 | $N_2$ - 4355.0 |

After reviewing all possible species from each of the three fuels, it was found that both $O_2^+$ and W were the most frequently identified species with three occurrences each in the first column of the possible species tables. Five other species appeared at least twice in the first column: $C_2$, OH, $CO^+$, $O_2$ and $H_2$. The multiple instances in which these species appeared support the fact that they were actually present.

Since previous testing using the Virginia Tech plasma torch with an argon-hydrogen feedstock, led to the identification of the presence of four atomic hydrogen lines, a series of focused scans was conducted near those wavelengths in an attempt to repeat the findings [9]. These tests did not yield conclusive results of the presence of any atomic hydrogen, however since methane was the primary fuel, and not a hydrogen-argon mixture, this is not an invalidating result. There was a slight detection of some light emitted near the 4341 Å, $H_\gamma$ atomic line, but the intensity was so slight that it was deemed unconvincing. However, looking back on the 30 SLPM methane test series, one of the possible species was the $H_\beta$ at 4861.33 Å, so the presence of atomic hydrogen cannot be counted out in hydrocarbon plasma.

## Final Remarks

The experimental tests results were positive in that there were definite peaks found which were very repeatable for methane, somewhat repeatable for ethylene and identifiable for propylene. Although the high flow rate/ high current methane tests resulted in what appeared to be slightly shifted peaks and different species present, more testing should be completed in order to verify this. In any event, similar species were found throughout all the tests, which indicates that these species are actually present. Even with the limited propylene test data, there were species found

that matched the more extensive methane and ethylene data. Also, the fact that argon was used as a carrier gas does not affect the spectrograpic results of propylene, since argon appears in wavelengths below the limits of both the PMT and monochromator.

## V. Theoretical Ignition Analysis

A complementary numerical study was conducted in an attempt to assess which species that are likely produced by a plasma torch might be effective in promoting ignition of hydrocarbons. Due to the high level of complexity involved in a plasma igniter system, it was not possible to generate a full kinetic model. Factors such as actual plasma temperature and the reaction scheme for excited species were unknown and had to be approximated. A similar analysis was conducted by Mitani [35], where the addition of O atoms was found to be 1.5 times as effective for ignition compared to the introduction of H atoms for hydrogen-air combustion. Results such as these give extra motivation to conduct a similar study to find out which species aid in ignition of hydrocarbons.

A NASA computer code entitled "A Hybrid Computer Program for Rapidly Solving Flowing or Static Chemical Kinetic Problems Involving Many Chemical Species" [36] was utilized to compute the chemical composition and ignition delay time of a methane-air reaction. The input file for this code was comprised of a simplified reaction list, as given in Appendix A, along with the initial temperature, pressure and composition of the mixture. It was noted that the $C_2$ radical was mentioned in the literature as being an easily identifiable radical, and also possibly occurred in the experiments, but was not in the reaction list. Further investigation determined that although $C_2$ is present in the majority of hydrocarbon-air reactions, and does radiate quite intensely, its omission from a chemical kinetics analysis has little effect on the accuracy of the results [37].

It is known that the electric arc does not completely fill the space between the anode and cathode, so only a fraction of the feedstock passing through the nozzle is broken down into more simple molecules, atoms and charged species. An equilibrium code, "Computer Program for Calculation of Complex Chemical Equilibrium Compositions, Rocket Performance, Incident and Reflected Shocks, and Chapman-Jouguet Detonations" [38], was used to determine the initial composition of the small percentage of the feedstock that was broken down. The input file for this code required two thermodynamic properties, such as temperature and pressure, and the chemical formula of the initial species, $CH_4$ in this case.

## Methodology and Results

The analysis technique used to simulate the torch started with running the chemical kinetics code for a series of initial mixture temperatures ranging from 1200 K to 1600 K to determine the species concentrations and ignition delay times for a stoichiometric $CH_4$-Air reaction. This "base" reaction is used as a point of reference to see if ignition delay time is increasing or decreasing with the addition of simulated plasma torch species.

The reaction was run for 2 ms, since if ignition does not take place within that amount of time, a real reaction would likely not occur [37]. As seen in Figure V.1, where the initial mixture temperature is listed on the right, the lower limit of ignition was found for test cases with initial

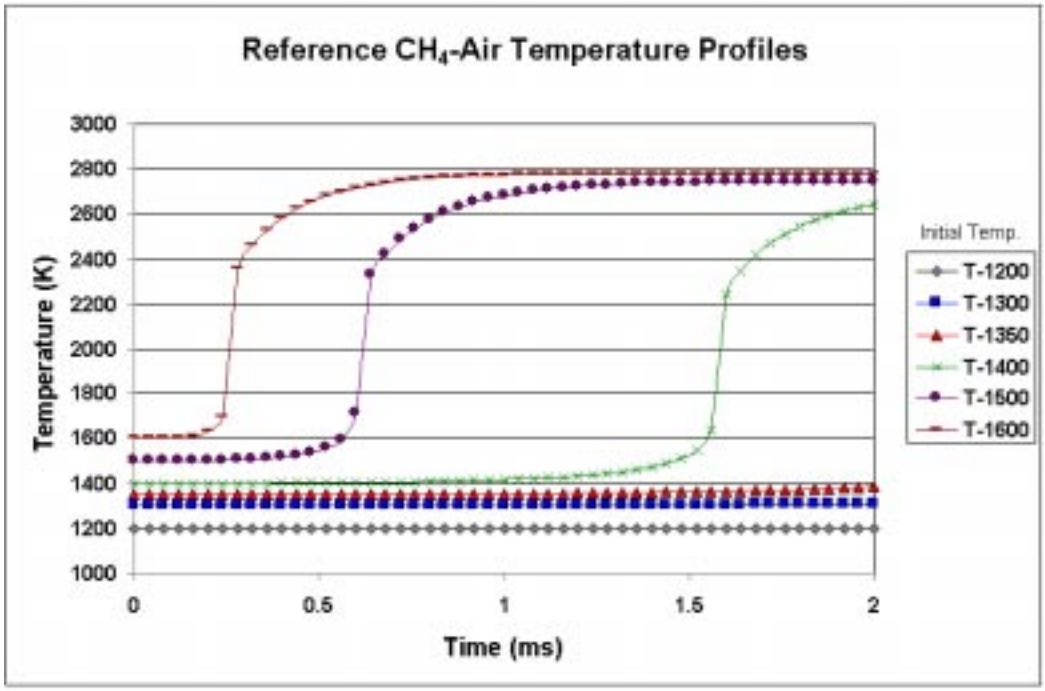


**Figure V.1: Stoichiometric Reaction**

mixture temperatures between 1375 K and 1400 K. Additionally, the decrease in delay time between 1400 K and 1500 K was nearly three times that of the decrease from 1500 K to 1600 K, which indicated that increasing the initial mixture temperature beyond 1600K would not significantly decrease ignition delay time. This verifies that enhancement of the reaction at lower temperatures could significantly decrease the ignition delay time, which is important in high-speed combustion.

Since the reaction scheme used in the kinetics code is an approximation to reality, and the least number of reactions that reasonably approximates reality is used, many of the species determined from the experiments are not present. These include all charged species, reactions involving nitrogen and reactions containing tungsten. Due to the observed absence of soot in the plasma torch exhaust, solid carbon was set as non-reacting within the code. With these restrictions, the species present in both the experimental data and kinetics code were H, OH, $H_2$, $O_2$ and $CO_2$. Nitrogen was present in the results of the code only because the initial input contained $N_2$ as part of the air composition, however the experimental results indicated that excited $N_2$ was present.

Since the plasma torch does not simply heat methane to some temperature, equilibrium compositions of methane at assumed elevated temperatures were taken to simply simulate the function of the plasma torch. The results of the equilibrium code for methane at various assumed temperatures are given in Figure V.2. It is interesting to note that both $C_2H_2$ and $H_2$ lose

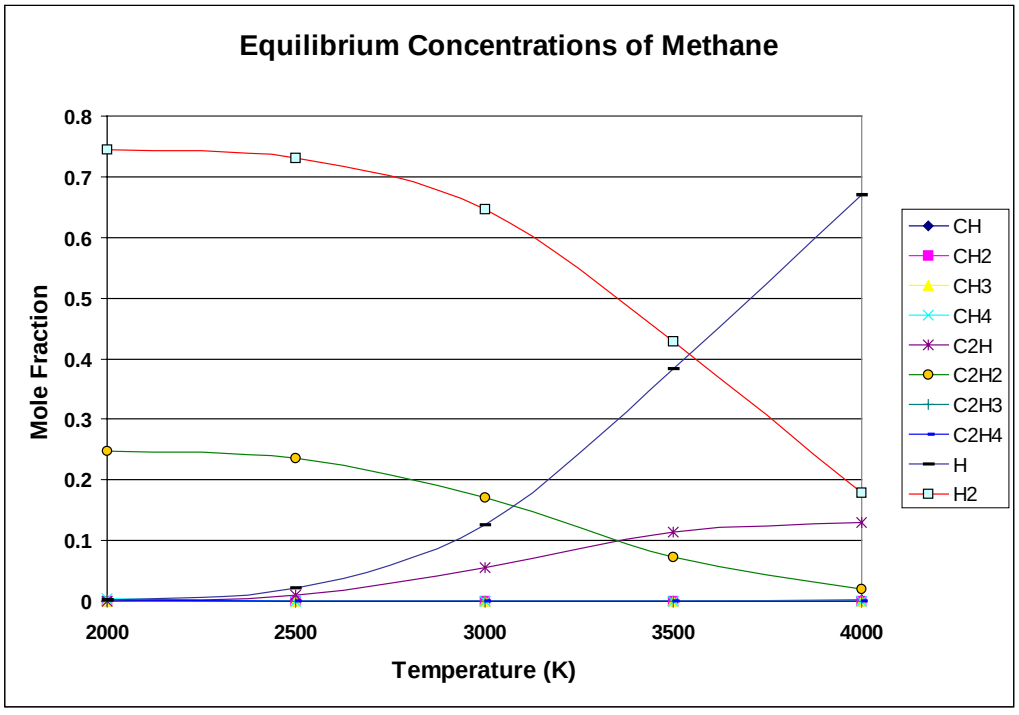


**Figure V.2: Equilibrium Concentrations of Methane**

hydrogen atoms to form $C_2H$ and monatomic hydrogen. In addition, the concentrations of all other species are essentially zero compared to these four. Again, as with the chemical kinetics

code there are no charged species present in the equilibrium code, therefore charged species have been omitted from this simulation.

The arc was arbitrarily assumed to break down 1% of the feedstock passing through the nozzle, therefore 1% of the initial methane composition in the input file of the chemical kinetics code was replaced with an equilibrium composition of methane at various elevated temperatures. For example, the stoichiometric value, by mole fraction, for methane-air reaction is:

$$\mathbf{0.2953\ CH_4 + 0.1476\ O_2 + 0.5571\ N_2 = 1.0000}$$

Now if 1% of the methane is replaced with the equilibrium composition of methane at, say, 3000 K then the initial composition would look like:

$$\mathbf{0.29235\ CH_4 + 1.6E\text{-}4\ C_2H + 5.1E\text{-}4\ C_2H_2 + 3.7E\text{-}4\ H + 19.1E\text{-}4\ H_2 + 0.1476\ O_2 + 0.5571\ N_2 = 1.0000}$$

Initial compositions such as the one given above were calculated for equilibrium composition temperatures ranging from 2000 K to 5000 K. It was determined through testing that above about 6000 K, the equilibrium composition does not change significantly and calculation of compositions above this temperature is wasted effort even though an actual plasma or arc temperature may be on the order of 10000 K.

The results for the ignition delay time, from the chemical kinetics code, for the simulated

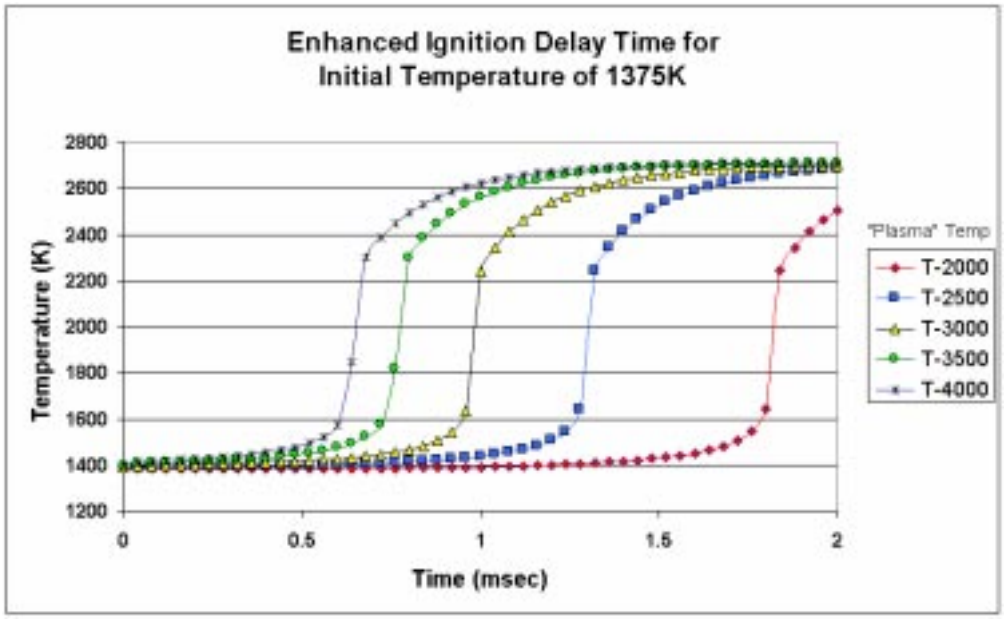


**Figure V.3**

(enhanced) plasma $CH_4$ input are given in Figure V .3. Each curve represents a 1% equilibrium concentration at the temperature indicated on the right, added to the 1375 K initial methane-air concentration.

The results indicate that the reference case at 1375 K which only "marginally" ignited, since it only increased in temperature to about 1600K, will now ignite and increase in temperature to above 2500 K with all the “enhanced” cases. Additionally, if the torch were producing the equivalent of 1% of equilibrium composition of methane at 4000 K, there would be about a 1.25 ms decrease in ignition delay time. This is important since faster reaction times are required for high-speed combustion applications. Also, even a “plasma” composition equivalent to the 2000 K methane equilibrium concentration is capable of igniting a fuel-air mixture that was previously considered unlikely to react.

To further test the simulated torch capabilities, the 1300 K case, which was clearly non-reactive in the reference cases, was run with the added equilibrium species. These results, given in Figure V.4, indicate that at lower temperature “plasma” equilibrium compositions, even the

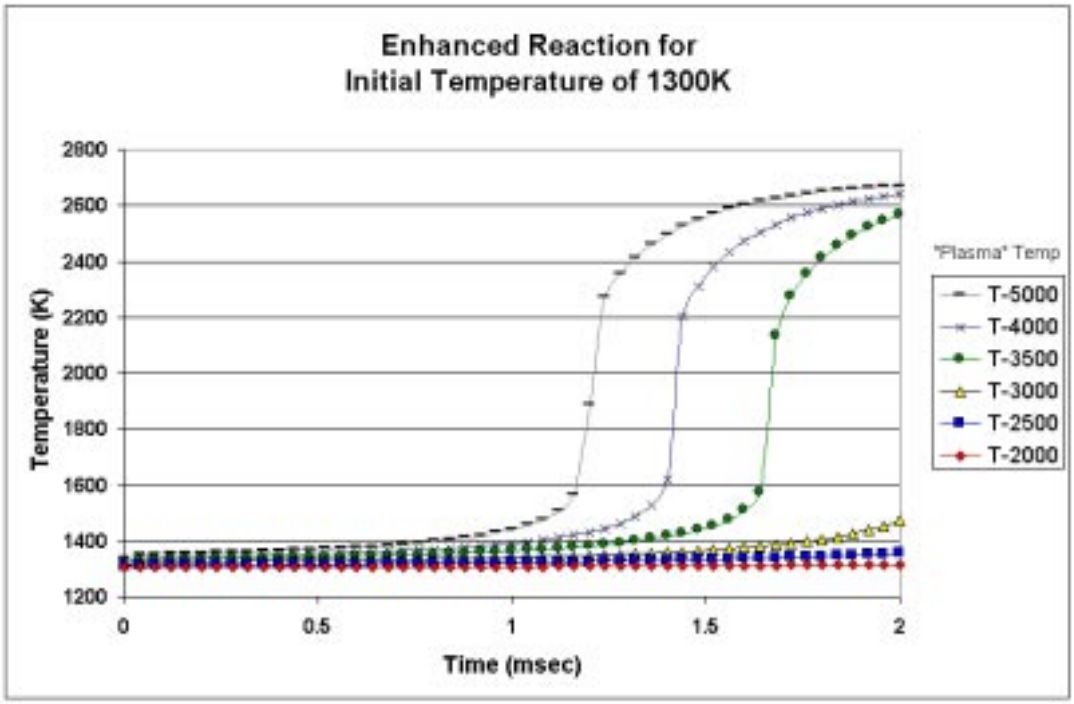


**Figure V.4**

enhanced input case would not ignite, but between 3000 K and 3500 K the equilibrium composition “plasma” species at these temperatures were enough to start combustion. This

result is also valuable since it shows that cases formerly non-ignitable may ignite if a methane plasma with a composition similar to that of equilibrium methane above 3000 K were present.

The enhanced input also had a definite impact on the final species present in the mixture after 2 ms. As an example, the concentrations of the species found in both the spectrometer experiments and kinetics code for the 1375 K case is given in Table V.1.

**Table V.1 - Effect of Enhancement on Species Production**

| | H | OH | $H_2$ | $O_2$ | $CO_2$ |
|---|---|---|---|---|---|
| Reference | 0.000175 | 0.000128 | 0.01909 | 0.15406 | 0.00047 |
| Enhanced | 0.015010 | 0.020800 | 0.02101 | 0.02671 | 0.04607 |

The enhanced case had an 82% reduction on the amount of $O_2$ present while increasing the OH concentration by 162%. A large increase in $CO_2$ was also attained, indicating that the $O_2$ is actually combusting and therefore producing stable species.

## Final Remarks

Due to the complexity of plasma torches and the chemical kinetics involved with them, the simplified simulation of the plasma through the use of methane equilibrium composition indicated that any amount of broken down methane supported combustion enhancement. This study, while not expansive, helped to determine that marginally and non-reacting mixtures of methane and air could be ignited, and ignited in a shorter amount of time, if broken down methane species are present in a mixture. As with many positive findings there is a limit to combustion enhancement with this approach in that beyond about 5000 K the equilibrium composition of methane does not change significantly and therefore at this temperature, only a minimum mixture temperature of about 1200 K can be ignited.

In addition, the theoretical analysis verified that certain species, such as H, OH, $H_2$, and $O_2$, could be present in the torch exhaust, and depending on what breakdown of methane is produced by the torch, the compositions of these species can vary. Furthermore, control of the amount of species produced by the torch through design changes might result in shorter ignition delay times and even promote ignition in otherwise non-reacting flows.

# VI. Conclusions

Efforts made to overcome plasma torch igniter problems using hydrocarbon feedstocks with the Virginia Tech plasma torch led to advances in both understanding how a plasma torch igniter operates and the effect the plasma has on combustion. Tests of the electrical properties of the torch, such as arc stability, voltage-current characteristics, arc gap influence and start capabilities, determined several characteristics. First, the arc appeared more stable at higher current settings for all fuels. Additionally, both methane and ethylene experienced unstable operation near 14 A. In observing the V-I characteristics, a correlation was found between the two. This led to the identification of two stable operating modes for methane (at 20 A and 40 A), but less defined operational modes using ethylene. Arc gap tests concluded that ethylene produced a much higher voltage gradient than methane. The start/restart tests concluded that within the confines of the test setup, the torch had 100% start and restart ability for both methane and ethylene.

Analysis of the physical properties of the torch determined that a high frequency starter, operating at low intensity, could significantly decrease or eliminate soot production. In addition, a small amount of high frequency signal was found to keep electrodes cooler and reduce electrode wear. Reduced electrode erosion is important since torch operation on hydrocarbon fuels increases the amount of electrode loss compared to operation with argon. High fuel flow rate, low current setting and more complex hydrocarbon feedstocks also promoted electrode cooling.

As the next step to operating the plasma torch with liquid fuels, a more complex hydrocarbon was tested. Propylene was found to be more prone to flameout and had higher amounts of electrode erosion than did methane or ethylene. The unstable operation was brought under control through the use of an argon carrier, which in turn reduced the power required to operate. The increased electrode loss may enhance combustion in scramjet applications due to the introduction of heated particles into the flow.

To obtain a more extensive “view” of how the torch is operating, audio and visual data was collected. Through the use of a microphone and high-speed CCD camera, a 180 Hz plasma jet oscillation was identified. Since the oscillation was traced back to the frequency of the power

supply, variation in power supply frequency will alter operational frequency. The ability to control such a variable could be used to reduce vehicle noise through wave cancellation. Pictures of the torch operation were also used to identify the source of gas leakage and when an obstruction was in the nozzle.

Analysis of the plasma and combustion plume through the use of emission spectroscopy and chemical kinetics computer code aided in the identification of combustion enhancing chemical species. Multiple experiments at identical control variables yielded similar results, hence showing repeatability of species present. Variation in feedstock type, while resulting in different peaks on plots of the spectrographic data, indicated that similar radicals were being generated regardless of hydrocarbon complexity. Chemical kinetics analysis demonstrated that a simulated torch plasma had a positive effect on ignition delay time, in that, at fuel-air mixture temperatures resulting in marginal or no ignition, the addition of modeled plasma for these cases induced ignition.

# Appendix A: Reaction List from NASA TM X-3403
# Hybrid Chemical Kinetics Program

The 82 reactions are listed on the left and the three values to the right are the A factor, N factor and activation energy (E) of the rate equation, respectively:

$$K=AT^{N-E/RT}$$

| | | | | | | | | |
|---|---|---|---|---|---|---|---|---|
| CH4 | + | O2 | => | CH3 | + | HO2 | 4.00E+13 | 0.0 | 56893. |
| H | + | CH4 | => | CH3 | + | H2 | 1.32E+04 | 3.0 | 8038. |
| O | + | CH4 | => | CH3 | + | OH | 9.03E+08 | 1.56 | 8485. |
| OH | + | CH4 | => | CH3 | + | H2O | 1.56E+07 | 1.83 | 2782. |
| HO2 | + | CH4 | => | CH3 | + | H2O2 | 9.00E+12 | 0.0 | 24641. |
| CH3 | + | O2 | => | CH3O | + | O | 1.32E+14 | 0.0 | 31400. |
| CH3 | + | O2 | => | CH2O | + | OH | 3.30E+11 | 0.0 | 8942. |
| H | + | CH3 | => | CH2 | + | H2 | 6.00E+13 | 0.0 | 15102. |
| H | + | CH3 | => | CH4 | | | 3.63E+23 | -3.29 | 2161. |
| O | + | CH3 | => | CH2O | + | H | 8.43E+13 | 0.0 | 0.000 |
| OH | + | CH3 | => | CH3O | + | H | 3.60E+13 | 0.0 | 0.000 |
| HO2 | + | CH3 | => | CH3O | + | OH | 1.80E+13 | 0.0 | 0.000 |
| CH3O | + | O2 | => | CH2O | + | HO2 | 4.03E+10 | 0.0 | 2126. |
| M | + | CH3O | => | CH2O | + | H | 1.90E+26 | -2.7 | 30602. |
| CH3 | + | CH2O | => | HCO | + | CH4 | 4.09E+12 | 0.0 | 8843. |
| CH3 | + | CH3 | => | C2H6 | | | 3.01E+38 | -7.81 | 8686. |
| CH3 | + | C2H6 | => | CH4 | + | C2H5 | 1.51E-07 | 6.0 | 6047. |
| H | + | C2H6 | => | C2H5 | + | H2 | 1.44E+09 | 1.5 | 7412. |
| O | + | C2H6 | => | C2H5 | + | OH | 1.00E+09 | 1.5 | 5803. |
| OH | + | C2H6 | => | C2H5 | + | H2O | 7.20E+06 | 2.0 | 865. |
| HO2 | + | C2H6 | => | C2H5 | + | H2O2 | 1.32E+13 | 0.0 | 20468. |
| | | C2H5 | => | C2H4 | + | H | 5.75E+14 | -0.874 | 35762. |
| C2H5 | + | O2 | => | C2H4 | + | HO2 | 1.02E+10 | 0.0 | -2186. |
| CH3 | + | C2H5 | => | C2H4 | + | CH4 | 1.14E+12 | 0.0 | 0.000 |
| H | + | C2H5 | => | CH3 | + | CH3 | 3.60E+13 | 0.0 | 0.000 |
| O | + | C2H5 | => | CH3 | + | CH2O | 1.12E+13 | 0.0 | 0.000 |
| OH | + | C2H5 | => | C2H4 | + | H2O | 3.00E+12 | 0.0 | 0.000 |
| M | + | C2H4 | => | C2H3 | + | H | 2.60E+17 | 0.0 | 96560. |
| M | + | C2H4 | => | C2H2 | + | H2 | 2.60E+17 | 0.0 | 79350. |
| CH3 | + | C2H4 | => | C2H3 | + | CH4 | 1.12E+12 | 0.0 | 0.000 |
| H | + | C2H4 | => | C2H3 | + | H2 | 5.40E+14 | 0.0 | 14904. |
| O | + | C2H4 | => | CH2O | + | CH2 | 3.46E+06 | 2.08 | 0.000 |
| OH | + | C2H4 | => | C2H3 | + | H2O | 2.00E+13 | 0.0 | 5942. |
| HO2 | + | C2H4 | => | C2H3 | + | H2O2 | 2.00E+12 | 0.0 | 17189. |
| | | C2H3 | => | C2H2 | + | H | 3.60E+42 | -9.265 | 49156. |
| C2H3 | + | O2 | => | CH2O | + | HCO | 5.40E+12 | 0.0 | 0.000 |
| H | + | C2H3 | => | C2H2 | + | H2 | 1.20E+13 | 0.0 | 0.000 |
| O | + | C2H3 | => | C2H2 | + | OH | 3.00E+13 | 0.0 | 0.000 |
| OH | + | C2H3 | => | C2H2 | + | H2O | 3.00E+12 | 0.0 | 0.000 |
| H | + | C2H2 | => | C2H | + | H2 | 6.00E+13 | 0.0 | 27820. |
| O | + | C2H2 | => | CH2 | + | CO | 2.17E+04 | 2.8 | 497. |
| OH | + | C2H2 | => | C2H | + | H2O | 6.00E+13 | 0.0 | 12917. |
| C2H | + | O2 | => | HCO | + | CO | 1.80E+13 | 0.0 | 0.000 |
| CH2 | + | O2 | => | CH2O | + | O | 2.45E+13 | 0.0 | 1490. |

```
CH2     +  H       =>   CH      +  H2          4.00E+13   0.0      0.000
CH2     +  O       =>   CO      +2 H           5.00E+13   0.0      0.000
CH2     +  CH3     =>   C2H4    +  H           4.20E+13   0.0      0.000
CH      +  O2      =>   HCO     +  O           2.00E+13   0.0      0.000
CH      +  O       =>   CO      +  H           4.00E+13   0.0      0.000
M       +  CH2O    =>   HCO     +  H           1.26E+16   0.0      77900.
CH3     +  CH2O    =>   HCO     +  CH4         4.10E+12   0.0      8843.
H       +  CH2O    =>   HCO     +  H2          2.30E+10   1.05     3280.
O       +  CH2O    =>   HCO     +  OH          4.15E+11   0.57     2762.
OH      +  CH2O    =>   HCO     +  H2O         3.40E+09   1.18     -447.
HO2     +  CH2O    =>   HCO     +  H2O2        3.00E+12   0.0      13076.
M       +  HCO     =>   H       +  CO          2.50E+14   0.0      16800.
HCO     +  O2      =>   CO      +  HO2         3.00E+12   0.0      0.000
H       +  HCO     =>   CO      +  H2          9.00E+13   0.0      0.000
O       +  HCO     =>   CO      +  OH          3.00E+13   0.0      0.000
O       +  HCO     =>   CO2     +  H           3.00E+13   0.0      0.000
OH      +  HCO     =>   CO      +  H2O         1.00E+14   0.0      0.000
OH      +  CO      =>   CO2     +  H           6.32E+06   1.5      -497.
HO2     +  CO      =>   CO2     +  OH          1.50E+14   0.0      23590.
CO      +  O       =>   CO2     +  M           5.30E+13   0.0      -4540.
H       +  O2      =>   OH      +  O           2.00E+14   0.0      16811.
O       +  H2      =>   OH      +  H           5.12E+04   2.67     6279.
OH      +  H2      =>   H2O     +  H           1.02E+08   1.60     3299.
OH      +  OH      =>   H2O     +  O           1.50E+09   1.14     99.
H       +  OH      =>   H2O     +  M           2.21E+22  -2.0      0.000
H       +  H       =>   H2      +  M           6.50E+17  -1.0      0.000
H       +  O       =>   OH      +  M           2.60E+16  -0.6      0.000
O       +  O       =>   O2      +  M           1.14E+17  -1.0      0.000
H       +  O2      =>   HO2     +  M           1.41E+18  -0.8      0.000
HO2     +  H       =>   OH      +  OH          1.68E+14   0.0      874.
HO2     +  H       =>   H2      +  O2          4.27E+13   0.0      1411.
HO2     +  O       =>   O2      +  OH          3.20E+13   0.0      0.000
HO2     +  OH      =>   H2O     +  O2          2.89E+13   0.0      -497.
HO2     +  HO2     =>   H2O2    +  O2          1.87E+12   0.0      1540.
H       +  H2O2    =>   H2      +  HO2         1.70E+12   0.0      3756.
H       +  H2O2    =>   OH      +  H2O         1.00E+13   0.0      3580.
O       +  H2O2    =>   OH      +  HO2         6.62E+11   0.0      3974.
OH      +  H2O2    =>   H2O     +  HO2         7.82E+12   0.0      1331.
OH      +  OH      =>   H2O2    +  M           2.21E+19  -0.76     0.000
```

## References


1. Curran, E.T., "Scramjet Engines: The First Forty Years", ISABE 97-7005, Sept. 1997.

2. Waltrup, P.J., White, M.E., Zarlingo, F., Gravlin, E.S., "History of U.S. Navy Ramjet, Scramjet, and Mixed Cycle Propulsion Development", AIAA 96-3152, 32nd AIAA/ASME/SAE/ASEE Joint Propulsion Conference, Lake Buena Vista, FL, July 1996.
3. Andrews, E.H., and Mackley, E.A., "Review of NASA's Hypersonic Research Engine Project", AIAA 93-2323, June 1993.

4. Northam, G.B., and Anderson, G.Y., "Supersonic Combustion Ramjet Research at Langly", AIAA 86-0159, Jan. 1986.

5. Rogers, R.C., Capriotti, D.P., and Guy, R.W., "Experimental Supersonic Combustion Research at NASA Langly", AIAA 98-2506, June 15-18, 1998.

6. Guy, R.W., Rogers, R.C., Puster, R.L., Rock, K.E., and Diskin, G.S., "The Nasa Langly Scramjet Test Complex", AIAA 96-3243, July 1-3, 1996.

7. Voland, R.T., etal., "Hyper-X Engine Design and Ground Test Program", AIAA 98-1532, April 27-30, 1998.

8. Timnat, Y.M., Advanced Airbreathing Propulsion, pp. 25-34, Krieger Publishing Company, Malabar, Florida, 1996.

9. Wagner, T., O'Brien, W., Northam, G.B., Eggers, J., "Plasma Torch Igniter for Scramjets", Journal of Propulsion, Vol. 5, No. 5, 1989.

10. Weinberg, F.J., "Ignition by Plasma Jet", Nature, Vol. 272, March, 1978.

11. V. Hruby, J. Kolencik, K.D. Annen, R.C. Brown, "Methane Arcjet Experiments," AIAA-97-2427, 28th Plasmadynamics and Lasers Conference, Atlanta, GA, June 23-25, 1997.

12. Albertson, C.W., and Andrews, E.H., "Mach 4 Tests of a Hydrocarbon Fueled Scramjet Engine", JANNAF Propulsion Subcommittee Meeting, CPIA Publication 639, Vol. 2, Dec. 1995.

13. Semenov, Y.S., and Sokolik, A.S., "Investigation of a plasma in Laminar and Turbulent Hydrocarbon Flames", Document ID 67N22442, Translated From Russian, June 30, 1966.

14. Fitzgerald, D.J., and Breshears, R.R., "Plasma Igniter for Internal Combustion Engine", Document ID 97N11405, NASA Pasadena Office, Oct. 31, 1978.

15. Cetegen, B., Teichman, K.Y., Weinberg, F.J., and Oppenheim, A.K., "Performance of a Plasma Igniter", SAE Automotive Engineering Exposition, Detroit, Feb. 25, 1980.

16. Northam, G.B., McClinton, C.R., Wagner, T.C., and O'Brien, W.F., "Development and Evaluation of a Plasma Jet Flameholder for Scramjets", AIAA 84-1408, June 11-13, 1984.

17. Orrin, J.E., Vince, I.M., and Weinberg, F.J., "A Study of Plasma Jet Ignition Mechanisms", 18th Symposium on Combustion, TCI, 1981.

18. Grove, E.L., ed. Analytical Emission Spectroscopy, Part I, Marcel Dekker, Inc., New York, 1972.

19. Perkampus, H.-H., Encyclopedia of Spectroscopy, Translated from German, VCH Verlagsgesellschaft mbH, D-69451 Winheim, 1995.

20. Grove, E.L., ed. Analytical Emission Spectroscopy, Part II, pp. 204-213, Marcel Dekker, Inc., New York, 1972.

21. Lago, V., de Graaf, M., Duten, X., Hulin, S., Dudeck, M., "Optical Spectroscopy and Probe Characterization of $N_2$-$CH_4$ Plasma Jets", AIAA 96-2302, 27th AIAA Plasmadynamics and Lasers Conference, New Orleans, LA, June 1996.

22. Röck, W., Auweter-Kurtz, M., "Spectral Measurements in the Boundary Layer of Probes in Nitrogen/Methane Plasma Flows", AIAA 97-2525, 32nd Thermophysics Conference, Atlanta, GA, June 1997.

23. Mawid, M.A., "Kinetic Modeling of Ethylene Oxidation in High Speed Flows", AIAA 97-3269, 33rd Joint Propulsion Conference and Exhibit, Seattle, WA, July 1997.

24. Smithells, Colin J., Tungsten, Its Metallurgy, Properties and Applications, Chemical Publishing Co., Inc. New York, 1953, pp. 209-210.

25. Hardy, T.L., "Electrode Erosion in Arc Discharges at Atmospheric Pressure," 18th International Electric Propulsion Conference, AIAA-85-2018.

26. Yih, Stephen W.H., Tungsten: Sources, Metallurgy, Properties and Applications, Plenum Press, New York, 1979, pp. 247-55, 266-70.

27. Stouffer, Scott, "Development and Operating Characteristics of an Improved Plasma Torch For Supersonic Combustion Applications," Masters Thesis, Virginia Polytechnic Institute & State University, July, 1989, pp. 14-19.

28. Howell, A.H., A.I.E.E. Trans., 58, 193, 1939.

28. Cobine, James Dillon, Gaseous Conductors, Theory and Engineering Application, McGraw-Hill Book Company, Inc. New York, 1941, pp. 167-8.

30. Wirth, Douglas A., "Soot Formation in Vitiated-Air Diffusion Flames," Masters Thesis, Virginia Polytechnic Institute & State University, June 1989.

31. Hura, H.S. and Glassman, I., "Soot Formation in Diffusion Flames of Fuel Oxygen Mixtures," Twenty-Second Symposium (International) on Combustion, The Combustion Institute, 1989.

32. Markusic, T.E., Spores, R.A., "Spectroscopic Emission Measurements of a Pulsed Plasma Thruster Plume", AIAA 97-2924, 33rd AIAA/ASME/SAE/ASEE Joint Propulsion Conference & Exhibit, Seattle, WA, July 1997.

33. Dean, J.A., Raines, T.C., ed., Flame Emission and Atomic Absorption Spectrometry, Vol. 3 – Elements and Matrices, Marcel Decker, Inc., New York, 1975.

34. Pearse, R.W.B., Gaydon, A.G., The Identification of Molecular Spectra, Chapman and Hall, London, 1976.

35. Mitani, Tohru, "Ignition Problems in Scramjet Testing", Combustion and Flame, Vol. 101, 347-359, Elsevier Science Inc, 1995.

36. McLain, A.G., Rao, C.S.R., modified by Jachimowski, C., "A Hybrid Computer Program for Rapidly Solving Flowing or Static Chemical Kinetics Problems Involving Many Chemical Species", NASA Report Number TM X-3403, July, 1976.

37. Personal conversation with Dr. Casimir Jachimowski of NASA Langly.

38. Gordon and McBride, "Computer Program for Calculation of Complex Chemical Equilibrium Compositions, Rocket Performance, Incident and Reflected Shocks, and Chapman-Jouguet Detonations", NASA SP-273, NASA Lewis Research Center, 1971.

# Vita

John Prebola was born in Kingston, Pennsylvania, on May 24, 1974. He moved to Sayreville, New Jersey in 1986 where he graduated from Sayreville High School in 1992 and attended North Carolina State University in the fall of that year. He completed his B. S. degree in Aerospace Engineering in the spring of 1997. John attended graduate school at Virginia Tech in the summer of 1997 where he conducted experimental research for his Master of Science degree in Aerospace Engineering.